



HAL
open science

High-temperature digital image correlation techniques for full-field strain and crack length measurement on ceramics at 1200°C: Optimization of speckle pattern and uncertainty assessment

Robert Kaczmarek, J.C. Dupré, Pascal Doumalin, Octavian Pop, Lucas Teixeira, Marc Huger

► To cite this version:

Robert Kaczmarek, J.C. Dupré, Pascal Doumalin, Octavian Pop, Lucas Teixeira, et al.. High-temperature digital image correlation techniques for full-field strain and crack length measurement on ceramics at 1200°C: Optimization of speckle pattern and uncertainty assessment. *Optics and Lasers in Engineering*, 2021, 146, pp.106716. 10.1016/j.optlaseng.2021.106716 . hal-03368828

HAL Id: hal-03368828

<https://hal.science/hal-03368828>

Submitted on 7 Oct 2021

HAL is a multi-disciplinary open access archive for the deposit and dissemination of scientific research documents, whether they are published or not. The documents may come from teaching and research institutions in France or abroad, or from public or private research centers.

L'archive ouverte pluridisciplinaire **HAL**, est destinée au dépôt et à la diffusion de documents scientifiques de niveau recherche, publiés ou non, émanant des établissements d'enseignement et de recherche français ou étrangers, des laboratoires publics ou privés.

High-temperature digital image correlation techniques for full-field strain and crack length measurement on ceramics at 1200 °C: optimization of speckle pattern and uncertainty assessment

Robert Kaczmarek ¹, Jean-Christophe Dupré ², Pascal Doumalin ^{2, •}, Octavian Pop ³, Lucas Teixeira ⁴, Marc Huger ¹

¹ IRCER, UMR CNRS 7315, Université de Limoges, CEC, 12 rue Atlantis, 87068 Limoges Cedex France

² Institut Pprime, UPR CNRS 3346, Université de Poitiers, 11 Boulevard Marie et Pierre Curie, 86962 Futuroscope Chasseneuil Cedex France

³ GC2D, Université de Limoges, 17 Boulevard Jacques Derche, 19300 Egletons Cedex France

⁴ Laboratoire Gabriel Lamé, Université d'Orléans, Université de Tours, INSA-CVL, 8 Rue Léonard de Vinci, 45072 Orléans

• Corresponding author

Highlights

- Preparation of optimized speckle pattern on ceramic samples for high temperature measurements
- Characterization of speckle patterns and evaluation of DIC uncertainty using a mechanical device at high temperature

- Improvement of DIC uncertainty by varying some DIC parameters and by using image pre-processing
- Measurement of crack length within refractories at high temperature by using 2P-DIC (2-Parts DIC)

Abstract

High-temperature mechanical tests coupled with Digital Image Correlation (DIC) on ceramics which exhibit rather low level of strain require to overcome extreme experimental conditions that usually can reduce significantly measurement accuracy. Thermal resistance of speckle pattern, black body radiation and heat haze are three main concerns, which should thus be taken into account while designing a high-temperature image acquisition setup. In this aim, an experimental procedure has been specifically designed in order to minimize the three above-mentioned disturbances. The main objective of this study is to select a suitable high-temperature resistant speckle pattern for mechanical characterization at 1200 °C (or above) on refractory ceramics. Most of tested speckle patterns were performed with white alumina adhesive and dark ceramic grains (silicon carbide or brown fused alumina). Different grain sizes of silicon carbide were tested. At first, different speckle patterns are compared in terms of DIC strain measurement uncertainty by discussing speckle features, some main DIC parameters and two image pre-treatments (low pass filter, image size reduction). Then, these speckle patterns are tested to analyse fracture behaviour of refractories through a Brazilian test. An enhanced digital image correlation technique (2P-DIC), dedicated to monitor the fracture behaviour, is applied to study the evolution of crack length. The best representation of crack progression has been achieved for sample surface covered with a fine SiC powder ranging from 50-100 μm . It is then possible to compare the fracture behaviour between

1200°C and 20°C and to show that the refractory exhibits more crack branching at 1200°C in comparison with behaviour at room temperature.

Keywords

Speckle pattern, Digital Image Correlation, Crack monitoring, Fracture behaviour, High temperature, Brazilian test, Refractory.

1. Introduction

Refractories are heterogeneous ceramics that are required in many industrial applications involving high temperatures (typically up to 1500°C) and corrosive environments to process essential daily life materials such as steel, non-ferrous metals, cement, and glass. These materials are often a result of complex formulations involving multiple natural or synthetic minerals in order to obtain the macroscopic physicochemical properties to fit the specifications required by each industrial application. In this regard, each application requires specific thermomechanical and thermochemical properties to ensure good operating conditions to process these daily life materials with a reasonable lifetime within the industrial process but also able to guaranty the safety of the plant and of the workers therein.

From a thermomechanical point of view, it is very important nowadays to identify constitutive laws of these heterogeneous materials at high temperature in order to model the behaviour of the industrial refractory linings in operative conditions. It is also very useful to study the relationship between the microstructure of these materials and the macroscopic thermomechanical properties in order to optimise the design of these microstructures. Indeed, given the highly heterogeneous microstructure of refractory materials, deviations from linear

elasticity are commonly observed as large grains combined with initial micro cracks lead, in many cases, to large non-linear mechanical behaviour (unlike most fine ceramic materials).

In order to characterise the thermomechanical behaviour of these refractory materials, stress strain curve should be ideally characterised during uniaxial loading, in tension and/or in compression. Since these kinds of experiments are very complex to manage accurately on ceramic materials at high temperature, an alternative solution is to manage non-uniaxial loading, for example diametrical compression combined with Digital Image Correlation (DIC). This very suitable combination allows the inverse identification of material parameters in tension and compression during monotonic loading as well as during creep. It can also allow to accurately monitor the fracture process development throughout the test.

The effectiveness of DIC for mechanical characterisation of materials is now well established in literature since it gives the opportunity to consider many “virtual extensometers” on any place of sample’s surface during loading, as well as to record fracture phenomena (such as crack branching). Indeed, the DIC techniques developed for many years are commonly used to study 2D surface deformations and have proved to be a powerful method to reveal the behaviour of materials [1-4]. DIC is based on the analysis of successive images of a specimen surface during a mechanical test. Local calculations based on degree of similarity of grey levels between the images corresponding to an initial state and to a deformed state result in a displacement field, which could be then recalculated to strain field. DIC technique has already been used to study the fracture behaviour of several materials [5-11]. The direct application of DIC process leads to an approximate assessment of cracks because the material transformation is assumed homogeneous across a DIC subset [12]. A solution consists in adapting the DIC process. The material transformation usually assumed homogeneous is thus changed: a subset can be split into two parts with different kinematics, each part being

separately treated by DIC [12-14]. Here we use our own adaptation of DIC for cracks monitoring named 2P-DIC (for 2 Parts DIC) [15] which is able to detect the presence of a crack, to measure its length and opening.

The performance of DIC is closely related to speckle pattern deposited on the sample surface [16-22]. Speckle pattern can be characterized by speckle size, distribution of grey levels [20] and grey level gradients [22, 23]. Image noise is another key parameter which can be reduced by applying a low pass filtering on raw images [24, 25]. High-temperature DIC tests (typically between 1000 and 1500 °C) require dealing with additional temperature-induced phenomena, such as heat haze, black body radiation and temperature resistance of speckle pattern. Table contains several records about successful high temperature DIC tests which can be found in the literature.

Heat haze can be described as an irregular flow of hot air between the camera and the sample, which causes variation of refractive index. This effect generates artefacts and loss of accuracy. It can be reduced by using: (i) a long integration time, causing noise averaging, with simultaneous application of neutral density filters [27, 28] for reduction of light intensity, (ii) a small fan between sample and camera [31, 32] to blow out the hot air and thus reduce heat haze in the measurement field. Black body radiation (temperature-induced electromagnetic radiation) modifies light intensity in function of temperature and has detrimental effect on speckle pattern contrast. It can be reduced by using: (i) a blue bandpass filter transparent for the wavelengths in a range of 440-460 nm, which are the least influenced by black body radiation from visible range, (ii) an additional illumination with a wavelength adjusted to the wavelength of bandpass filter. Temperature resistance of speckle pattern must be high enough, so that the hypothesis of optical flux conservation used by DIC is satisfied during all the targeted high temperature mechanical test. Different solutions can be found in literature,

as shown in Table 1. It can be ensured using: (i) a high temperature resistant material applied by plasma spraying technique [27] through a grating in order to reinforce contrast, (ii) a high-temperature resistant inorganic adhesive mixed with a high temperature resistant powder, (iii) the natural speckle pattern of the sample resulting from initial material's microstructure [33].

Table 1. Summary of a bibliographical review about high-temperature DIC experiments

Specimen	Testing temperature	Reduction of black body radiation	High temperature resistant speckle pattern	Resolution [$\mu\text{m}/\text{pixel}$]	Avg. speckle size [μm]	Year [Ref]
Stainless steel	1200°C	Blue bandpass filter	Black cobalt oxide blended with commercial high-temperature inorganic adhesive	58	-	2010 [26]
Carbon fiber	2600°C	Blue bandpass filter	Plasma sprayed tungsten coating	-	-	2014 [27]
Zirconium silicate	1350°C	Blue bandpass filter	Silicon carbide powder	16	6*16=96	2015 [28]
Stainless steel	1150°C	Blue bandpass filter	White yttria-based and black silica-based ceramic paints	26	-	2016 [29]
Stainless steel	900°C	Blue bandpass filter	White yttria-based and black silica-based ceramic paints	20	50	2017 [30]

Therefore, the present paper deals with the development of a dedicated experimental protocol: suitable sample surface preparation, optimised conditions for images acquisition, characterisation of speckle patterns and choice of some DIC parameters and image pre-processing. This experimental protocol should allow to obtain the adequate optical precision compatible with quite low level of strains within the elastic domain of these refractory materials and also compatible with the early crack progression observation before final rupture of the sample, despite the different sources of disturbance involved by high temperature.

2. DIC Methods

2-1. Measurement techniques: DIC and 2P-DIC

Digital Image Correlation consists in recording two digital images of two different mechanical states: a reference state and a deformed state. The DIC process used in this work [12] consist in locally matching images of the sample surface at initial and final mechanical states. A series of subsets D (with a size of $m \times n$ pixels²) defined on a regular grid (constant spacing on the zone of interest) in the initial image is used for this matching. A local material transformation ϕ_a between the two images is defined at least by two components of displacement (u, v) , nevertheless four components of local gradients can be added depending of the studied mechanical problem. On each subset D , the unknown values $\underline{q} =$

$\left(u, v, \frac{\partial u}{\partial x}, \frac{\partial u}{\partial y}, \frac{\partial v}{\partial x}, \frac{\partial v}{\partial y}\right)$ are calculated from the smallest value of the correlation coefficient C .

$$C(\underline{q}) = \sum_D c^2(\underline{q}) \text{ with } c(\underline{q}) = \left[\frac{f(\underline{x})}{\langle f \rangle} - \frac{g(\phi_a(\underline{x}))}{\langle g \rangle} \right] \quad (1)$$

where f and g represent the grey levels of pixels, $\langle f \rangle$ and $\langle g \rangle$ are their averages in D and $\phi_a(D)$, \underline{X} and \underline{x} are the coordinates of grey levels for the reference and the deformed state respectively. The best solution \underline{q} is obtained from a least-square minimisation and an iterative Newton scheme. Subpixel bilinear interpolation of grey levels of the deformed image is used to achieve subpixel displacement measurement. To avoid detection ambiguity, a random distribution of grey levels (speckle pattern) is used and artificially made on sample surface as presented after. We assume that grey level distribution follows strain of material (conservation of the optical flow). From the displacement field obtained by DIC process, the strain field is calculated by finite differences scheme [21]: the local strains E_{xx} , E_{yy} , E_{xy} are evaluated from displacements of four neighbouring points (four centers of the neighbouring subsets) on the grid of DIC. In this case, the gauge length is equal to the distance between two neighbouring subsets (L_0).

2P-DIC is an extension of the usual DIC process. It consists in allowing of the subset D to split at the position X_C in two parts D_1 ($x < X_C$) and D_2 ($x > X_C$) as shown in Figure 2 with an orientation θ of the boundary [15, 34]. The expression of the correlation coefficient (1) becomes:

$$C_{XC}(X_C, \theta, \underline{Q}) = \sum_{D_1} c^2(\underline{q}_1) + \sum_{D_2} c^2(\underline{q}_2) \quad (2)$$

with $\underline{q}_i = \left(u_i, v_i, \frac{\partial u_i}{\partial x}, \frac{\partial u_i}{\partial y}, \frac{\partial v_i}{\partial x}, \frac{\partial v_i}{\partial y} \right)$ the vector of material transformation parameters in the part D_i ($i=1,2$). The vector \underline{Q} represents the gathering of two vectors \underline{q}_1 and \underline{q}_2 . The matching consists in searching the best values of X_C , θ and \underline{Q} which minimize $C_{XC}(X_C, \theta, \underline{Q})$. For each value of X_C varying by one-pixel step from $-m/4$ to $m/4$ and h varying between -50° and 50° with a pitch of 10° , the same minimization process for standard DIC is used to achieve a best estimation of \underline{Q} .

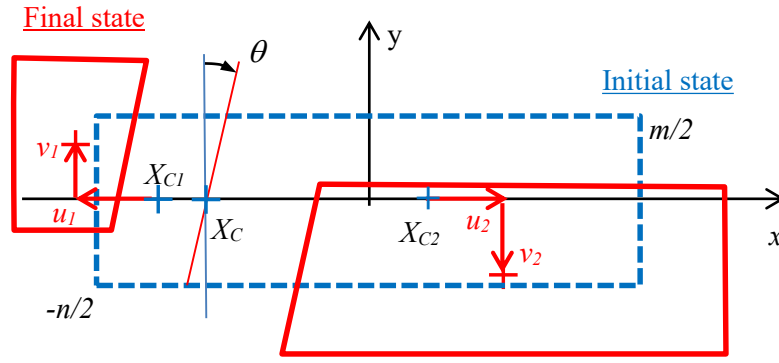


Figure 1 : Principle of the 2P-DIC, decomposition of a subset.

The detection of a crack is obtained with the calculation of a pseudo strain within each subset:

$$\varepsilon = \frac{\sqrt{(X_{C2} - X_{C1} + u_1 - u_2)^2 + (v_2 - v_1)^2}}{|X_{C2} - X_{C1}|} - 1 \quad (3)$$

When this pseudo strain value is higher than a threshold value ε_{Thres} , a discontinuity is detected in D . ε_{Thres} is defined as the maximal value between strain measurement uncertainty and experimental strain for which diffuse cracking starts. Here the value of strain measurement uncertainty is unfortunately, in most of cases, higher than the starting point of diffuse cracking, thus ε_{Thres} will be directly given by strain measurement error.

2-2. Uncertainty assessment

In term of speckle pattern optimisation for high temperature investigations and associated treatments, 2P-DIC and DIC use the same minimisation algorithm and interpolation, therefore their performances regarding quality of surface preparation are quite similar. Thus, in a first step, only the DIC technique will be used here to choose the best speckle pattern among the different proposed sample preparations, *i.e.* the one, which will give the best measurement accuracy. In literature [19-22, 35], several studies have already demonstrated the link between

displacement uncertainty and speckle pattern properties. In addition to speckle size and grey level histogram which are well known to play a key role in quality of DIC measurements, the standard deviation uncertainty of the displacement measurement in the x axis direction (σ_{U_x}) is in fact inversely proportional to the subset size in the direction of the displacement (m) and to the root of the average of squared grey level gradients ($\sqrt{\nabla g^2}$) and proportional to the standard deviation of the image noise (σ_n). It can be expressed by:

$$\sigma_{U_x} \propto \frac{\sigma_n}{\left[m \cdot \sqrt{\nabla g^2} \right]} \quad (4)$$

That is why the main features of our speckles, described by grey level histogram, grey level gradients, and speckle size will be discussed. Grey level histogram will be characterized by standard deviation of grey levels (σ_{GL}). In order to quantify contrast, the image will be derived in horizontal direction (properties are assumed isotropic) and the root of the average of squared grey level gradients $\sqrt{\nabla g^2}$ will be calculated [34]. Speckle size can be estimated from the full width at half maximum of autocorrelation curve [20]. From theoretical point of view for a binary image (black particles on a white background) and for the case of particles of same geometry, this width exactly corresponds to the size of the particles. For grey level images (rather dark particles having several grey levels on a white background), this width gives a good approximation of particles size [36, 37].

Low pass filter (Gaussian filter with a size of 3x3 pixels) is commonly used to decrease DIC uncertainty [24, 25]. Indeed, such a filter decreases the random noise mainly coming from the camera (i.e. standard deviation of the noise σ_n) but also grey level gradients (i.e. $\sqrt{\nabla g^2}$).

Usually σ_n decreases much more than $\sqrt{\nabla g^2}$. As displacement uncertainty is proportional to the

ratio $\sigma_n/\sqrt{\nabla g^2}$ with our images. Uncertainty has been assessed by preliminary tests, simply by studying the deformations of the investigated refractory sample in real environmental measurement conditions just before any loading (strain is thus assumed to be zero). Performances of strain measurements with these assumed stable conditions have been characterized by measuring the standard deviation of tension-compression deformations (σ_{Exx} or/and σ_{Eyy}) evaluated on sample surface during a given period of time (typically 60 min before loading). This protocol has been chosen instead of displacement assessment because calculation of strain allows us to directly eliminate the in-plan rigid displacements which appear in this study at high temperature (see next section). Furthermore, in small deformation hypothesis, strain and displacement uncertainties are linked to the distance between two used subsets (L_0) and the relation can be simply expressed by:

$$\sigma_{Exx} = \frac{\sigma_{Ux}}{L_0} \quad (5)$$

3. Experimental methods

3-1. Mechanical device for Brazilian test

The experimental device that has been used consists in one part dedicated to image acquisition and another part dedicated to mechanical loading at high temperature. The optical image acquisition setup, presented on Figures 1a and 1b, has been specifically designed taken into account most of critical points mentioned previously from bibliographic review. It consists of a high-resolution camera (PROSILICA GX 6600 - 6576x4384 pixels), a lens (AF Micro-Nikkor 200 mm f/4D IF-ED), two high power panels of LED (LINKSTAR LED VD-416D-K2 with colour temperature of 5500 K) to light the sample (with enough blue light radiation on the overall sample surface), a blue bandpass filter (MIDOPT BP470) with the

wavelengths in a range of 425-495 nm (reducing the influence of black body radiation), two fans (one cooling the camera, one blowing out hot air from hot surface of the furnace window - reducing heat haze) and a furnace with a transparent window made of glass ceramic. Images are recorded with a resolution of 0.014 mm/pixel.

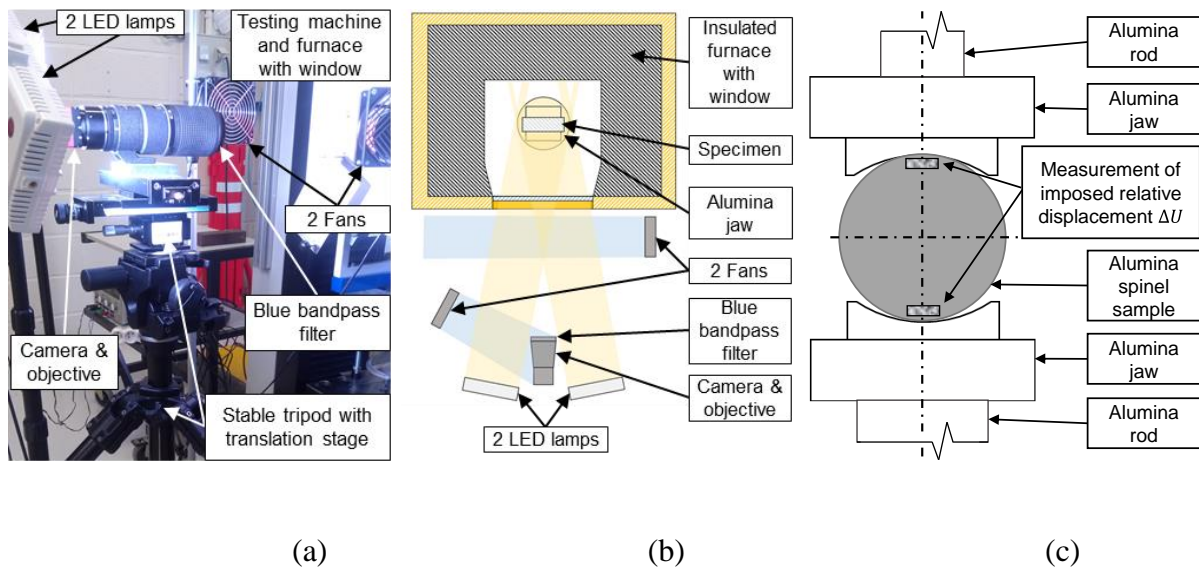


Figure 2: Testing setup for Brazilian test at high temperature: (a) real image of experimental setup, (b) drawing of experimental setup for images acquisition (c) drawing of Brazilian test setup.

Figure 1c shows a drawing of the mechanical test. Samples are circular disks (diameter 50 mm), which are loaded under compression against two alumina jaws with a circular shape for better contact with sample. This Brazilian test system is placed in a INSTRON 4507 testing machine. Compression loading is vertically applied with a rate of 0.05 mm/min and a cell (capacity of 5 kN) measures the load level. The relative displacement ΔU imposed by the two alumina jaws is measured directly on the sample (removing contact effects) by DIC as the difference between displacements of two zones (128x32 pixels) placed at the top and at the bottom of sample (see Figure 1c). A dedicated furnace (maximum temperature of 1250°C) is

mounted on the testing machine and allows the free vertical translation of the alumina rods used to apply the load on the sample through of alumina jaws.

3-2. Samples and speckle pattern preparation

A same fired alumina-spinel refractory brick has been used for all tests of speckle patterns presented here. This refractory material for steel making is typically industrially fired at very high temperature (about 1700°C), which is much higher than the temperature considered in the present study (1200°C). Therefore, it is reasonably supposed that the material will remains stable at the investigated temperature.

Dimensions of circular disc shaped specimens machined for Brazilian test have been selected in relation to maximal grain size [37] and thickness (Th_{Sample}) to diameter (D_{Sample}) ratio suggested for rocks [38] and sintered specimens [39]. Taking into account the above-mentioned points, specimen dimensions for indirect tensile test were: D_{Sample} 50 mm x Th_{Sample} 12.5 mm.

Alumina jaws, with specimen to jaws (D_{Jaws}) diameters ratio of $\rho = \frac{D_{Sample}}{D_{Jaws}} = 0.67$ [40], are used to assure correct stress distribution within the central area of the disc with reduction of stress concentration at the contact between sample and jaws.

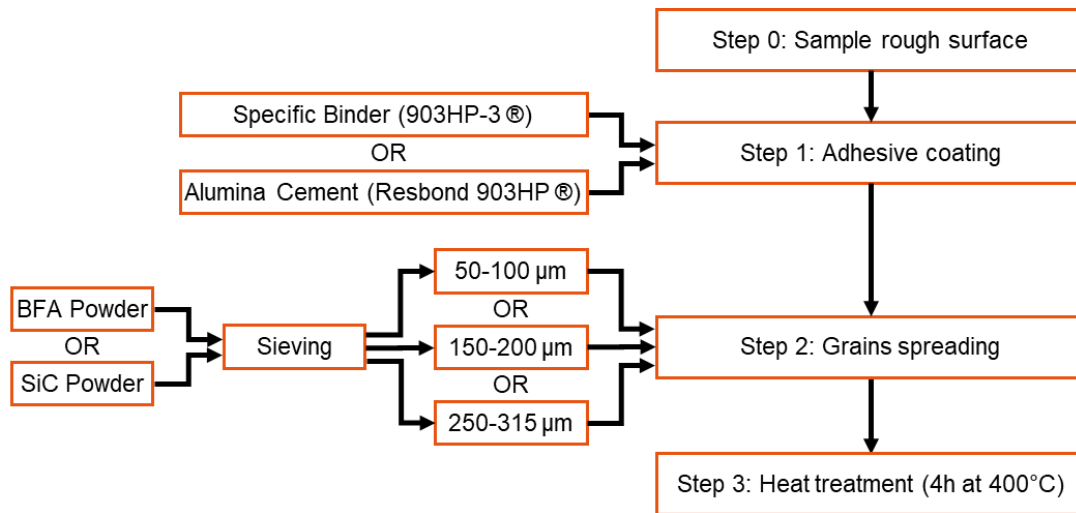


Figure 3. Block diagram describing speckle patterns preparation on sample surface.

A block diagram explaining speckle patterns preparation procedure is presented on Figure 3. All samples and their main features are given in Table 2. Sample reference, presented in this Table 2, consists of three main data separated with underscores: (i) Information regarding application of an adhesive coating which can be a white alumina cement “C” (commercial product named Resbond 903HP Ceramic Adhesive with maximum application temperature of 1790°C) or specific binder “B” (liquid component of the alumina cement); (ii) Grains that constitute the speckles, where “SiC” stands for Silicon Carbide and “BFA” for Brown Fused Alumina; (iii) Grain size range resulting from powder sieving above sample surface.

Table 2. Samples references with speckle pattern characteristics.

Sample reference	Adhesive coating	Powder type	Grain diameter [μm]
B_SiC_50-100	Specific binder	SiC	50-100
C_SiC_50-100	Alumina cement	SiC	50-100
C_SiC_150-200	Alumina cement	SiC	150-200
C_SiC_250-315	Alumina cement	SiC	250-315

The reasoning supporting usage of an adhesive coating is to provide a strong adhesion between tested samples and dark ceramic particles spread on the surface (especially important for bigger particles), as well as to increase contrast with dark speckles. The studied speckles types presented here have been specifically chosen to exhibit different grain sizes (in comparison to pixel size) and different contrast (in comparison to background surface colour). A particular attention has been also paid to choose grains compositions that could be thermodynamically rather stable in the all temperature range of our experiments.

3-3. Thermal cycle

Managing accurate measurements at high temperature requires to follow a well-established experimental protocol described in Figure 4. After preloading the sample at 50 N at room temperature, a ramp of 5 hours is necessary to reach the 1200°C in the oven required for the high temperature Brazilian test. Then, in order to avoid any parasitic displacements of loading parts, an idle time of 40 minutes is firstly respected for temperature equalization around the sample. Then, the study of uncertainty is managed during 60 minutes, in force-controlled mode with the same preload of 50 N. Such very low level of preload guaranties that no creep can occurs a 1200°C with such high refractory material. Then, Brazilian test is performed in displacement-controlled mode with a vertical compressive displacement rate of 3 mm/h (0.05 mm/min), and this final step last for about 20 mm when sample is broken. For the stability test and during the Brazilian test itself, images were acquired with an acquisition rate of 1 picture per second.

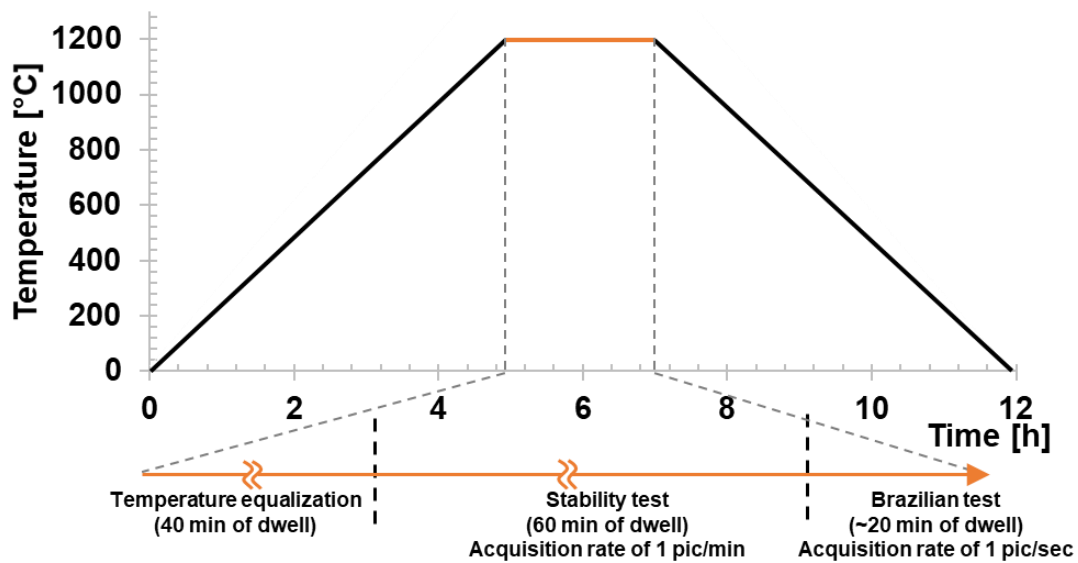


Figure 4: Thermal cycle (heating/cooling rate of 5°C/min, maximal temperature of 1200°C) with detailed testing procedure during dwell time.

4. Results and discussion

4-1. Main speckle pattern features

4.1.1. Grey levels histograms and contrast

For each of the five investigated speckle patterns, an example of pictures acquired at 1200°C during the stability test is presented on Figure 5. An enlargement of the central part and the grey level histogram (pixel occurrence versus grey level) of a large zone inside the sample are shown. One can observe that the background corresponding to sample has a high grey level, larger than 128 and speckle particles are darker. Although experimental conditions have been optimised to acquire bright, but not saturated images. Little saturation part is related with reflections of SiC particles. Pictures exhibit a relatively high contrast between adhesive coating and particles. This observation is confirmed by the shape of histograms on Figure 5

and values of grey level standard deviations resumed in Table 3. Grey levels are not distributed on the full range of images (256 grey levels) but only on the upper half, and thus pictures appear as rather bright. This global brightness is clearly linked to the high temperature of the sample (1200°C) which unfortunately result in black body radiations with a significant contribution in the visible spectrum acquired by the optical camera. Despite the used of an external blue light, the blue bandpass filter does not eliminate all black body radiations which contribute to increase the average grey level of the images.

Undoubtedly, this distribution of grey levels on a small part upper of the range leads also to rather small greyscale standard deviation and to rather small grey level gradients which both drives the measurement uncertainty (formula 4).

The values of $\sqrt{\nabla g^2}$ in Table 3, around of 5 grey level pixel⁻¹, are smaller than the ones which can be obtained at room temperature (13 grey level pixel⁻¹). Thus, DIC uncertainty will be larger during tests at 1200°C. C_SiC_50-100 gives the highest value of $\sqrt{\nabla g^2}$ with 5.6 grey level pixel⁻¹ according to other patterns ($\sqrt{\nabla g^2}$ between 4 to 4.3) but these differences remain weak. The analysis of experimental measurement accuracy (presented after) will permit to prove if these discrepancies are significant.

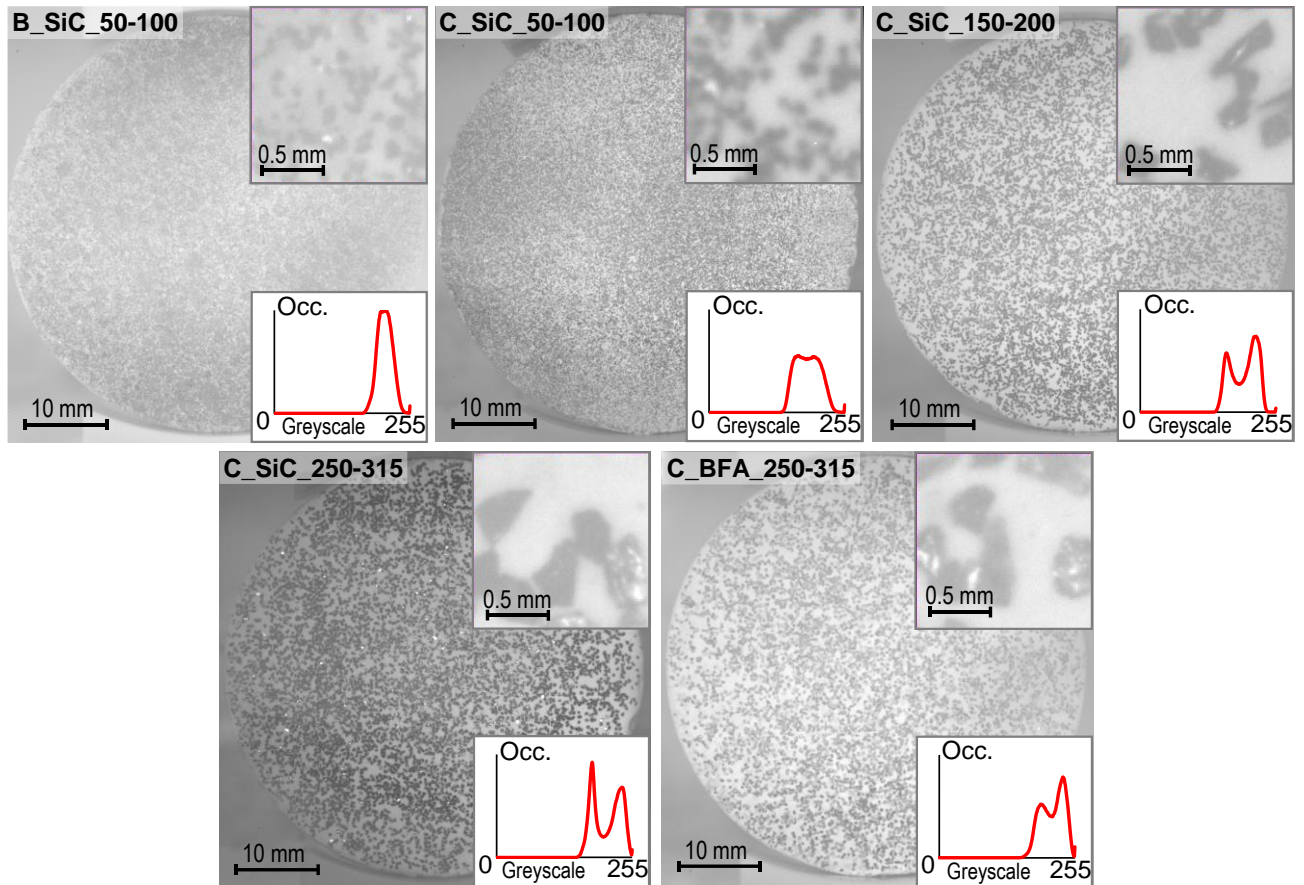


Figure 5: Pictures of different patterns at 1200°C in full resolution (0.014 mm/pixel), enlargement x15 (on top right), grey level histogram (on bottom right).

Table 3: Main speckle features at 1200°C with full resolution without any filter.

	Std. dev. of grey levels σ_{GL}	Average grey level gradient $\sqrt{\nabla g^2}$ (pixel ⁻¹)	Speckle size (pixel)	
			From Sieve size	From Autocorrelation curves
B_SiC_50-100	13.0	4	3.50-7.00	10
C_SiC_50-100	24.1	5.6	3.50-7.00	13

C_SiC_150-200	24.5	4.3	10.50-14.00	20
C_SiC_250-315	25.5	4	17.50-22.05	28
C_BFA_250-315	21.9	4.24	17.50-22.05	24

4.1.2. Speckle size

From Figure 5, one can also observe the different particles sizes that have been considered to constitute each tested speckle pattern, from the smaller ones to the bigger ones. The shapes of BFA or SiC particles are not regular and are not spherical. In addition, despite a great attention paid during the manufacturing of patterns, the spatial distribution of the particle is not perfectly uniform within the overall surface of the sample (existence of some agglomerated particles and some small areas without any grain). As previously explain, autocorrelation curves presented on Figure 6, allows to estimate size of the speckle from the value of full width at half maximum. These estimated values are reported in last colon of Table 3. One can observe that autocorrelation results (Table 3: column 4) give higher values (about 1.5 to 2 times higher) than particle size coming from sieving (Table 3: column 3). Even if the 2 ways to estimate size could lead intrinsically to some differences, this result could also come from particle agglomerations already mentioned.

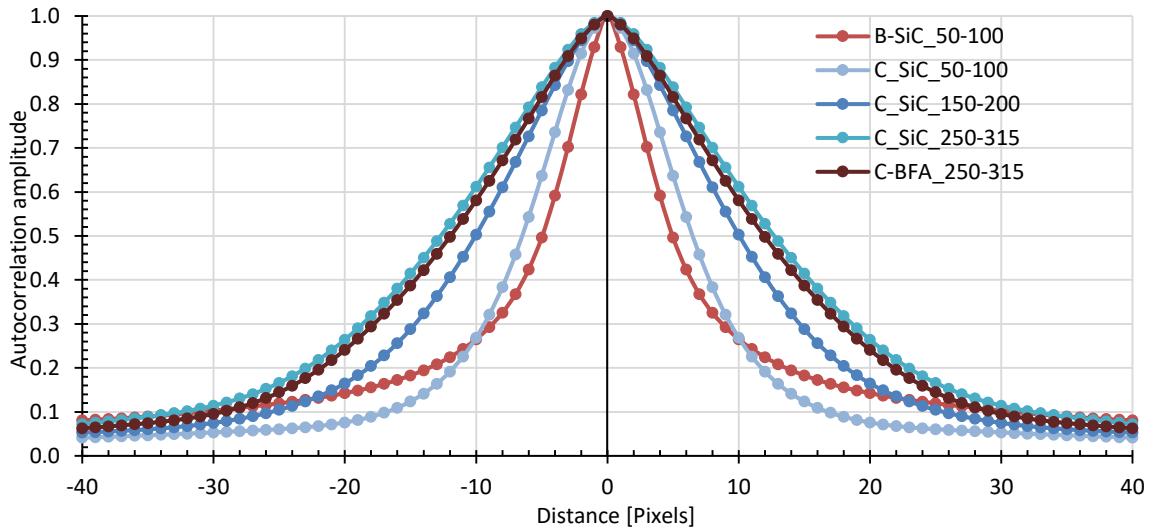


Figure 6: Autocorrelation curves for different speckle patterns measured at 1200°C.

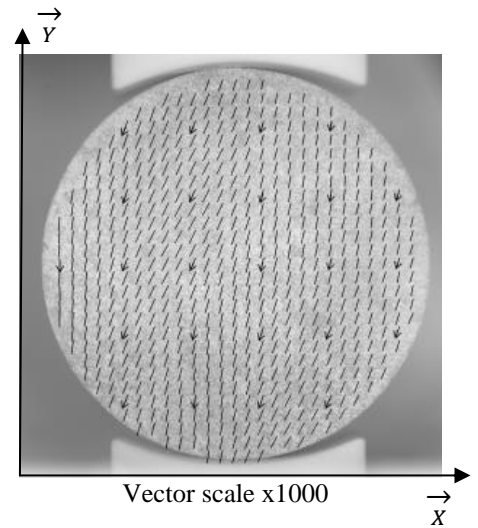
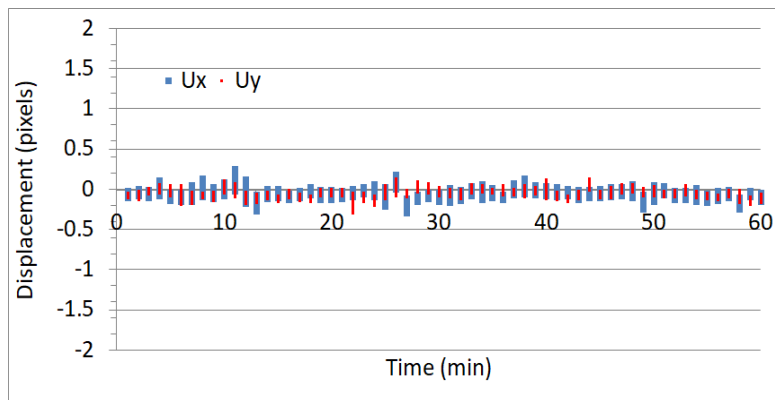
At this stage, only considering geometrical characteristic of speckle patterns, one can state:

- from contrast point of view, C_SiC_50-100 could be the most valuable speckle with highest value of average grey level gradient (5.6 pixel^{-1}) with rather small speckle size (13 pixel). But difference of average grey level gradient between considered speckle remains weak;
- from speckle size point of view of point of view, B-SiC_50-100 could be the most valuable speckle with lowest value of speckle size (10 pixel) with reasonable value of average grey level gradient (4 pixel^{-1}).

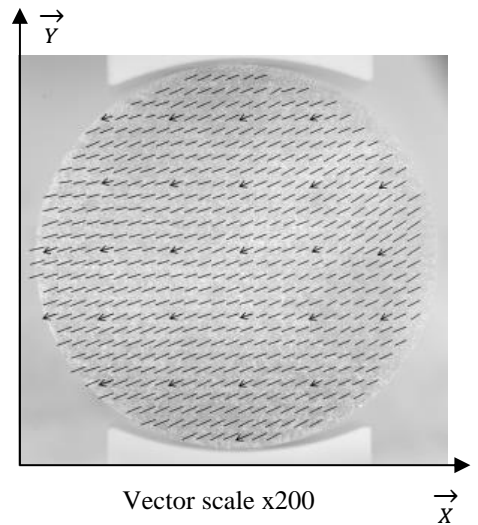
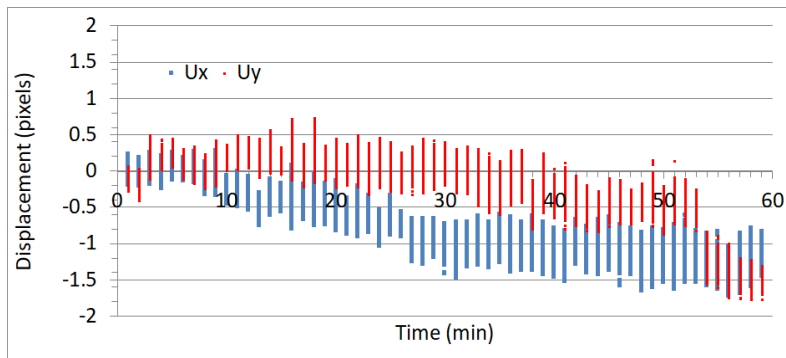
4-2. High temperature effects: preliminary tests

Even if the target of this work is to optimize the experimental protocol for accurate measurements at high temperature (eg 1200° C in current study), it could nevertheless be very useful to show some results obtained with exactly same experimental protocol at room

temperature (much easier measurement conditions). Thus, Figure 7 presents evolution of horizontal (UX) and vertical (UY) displacements for all subsets versus time at room temperature (as reference) and at high temperature (1200°C) in the case of B_SiC_50-100 . Only this case is presented here since similar trends have been observed for all other cases. At 20°C, U_x and U_y displacements are very stable around zero value with quite small variations during all the 60 min duration of this stability test. At high temperature, both U_x and U_y global displacements deviate versus time from initial position and larger spectrum of variations could be observed at each state (within each acquired image). Indeed, for exactly same speckle preparation, room temperature acquisition offers much easier measurement conditions (larger Std. dev. of grey levels $\sigma_{GL}=18.1$ and larger Average grey level gradient $\sqrt{\overline{I^2}}=13$) than the ones at 1200°C ($\sigma_{GL}=13$ and $\sqrt{\overline{I^2}}=4$). This intrinsic alteration of images features easily explains the larger spectrum of variations which could be observed for each state at high temperature. About U_x and U_y global displacements deviation, it is interesting to visualise displacement vector orientation (right of Figure 7a, b). After 1h at 20°C and after 1h of dwell at 1200°C, displacement fields on sample surface are uniform with almost the same direction but with a ten times smaller range at 20°C (about 0.25 pixels means 3.5 μm at 20°C, about 2.5 pixels means 35 μm at 20°C). These observed movements are most probably caused by the thermal expansion of camera support (tripod), which generate a global and progressive movement (upward and right) of the camera with a slight increase of temperature within the room due to heat flux coming from the furnace at high temperature. This global and progressive movement of the camera results in negative values of U_x and U_y global displacements for the vectors on sample. All tripod legs being probably not equally exposed to temperature rise, the observed movement on the sample is not perfectly vertical.



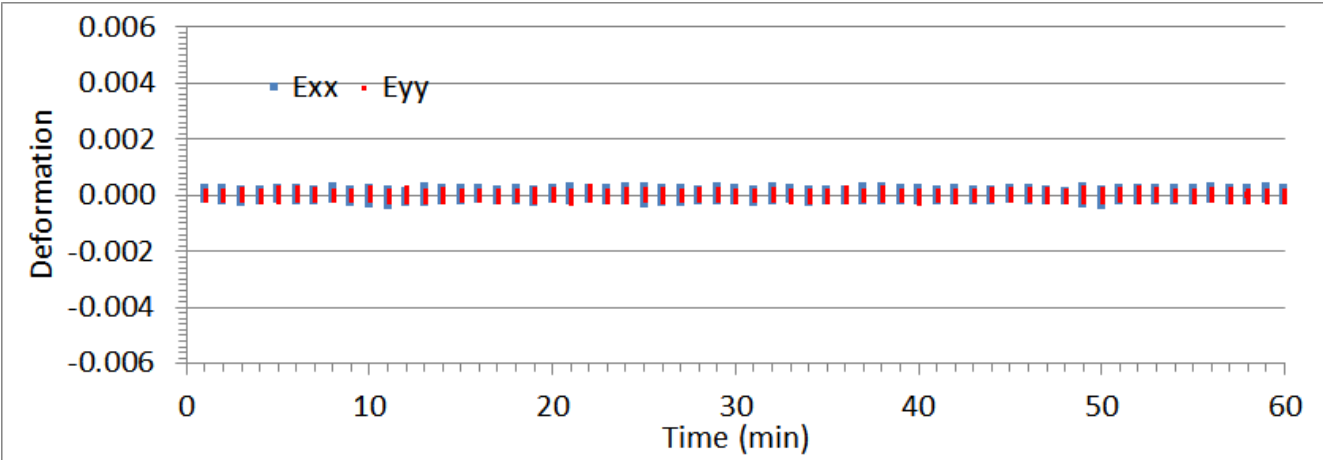
(a)



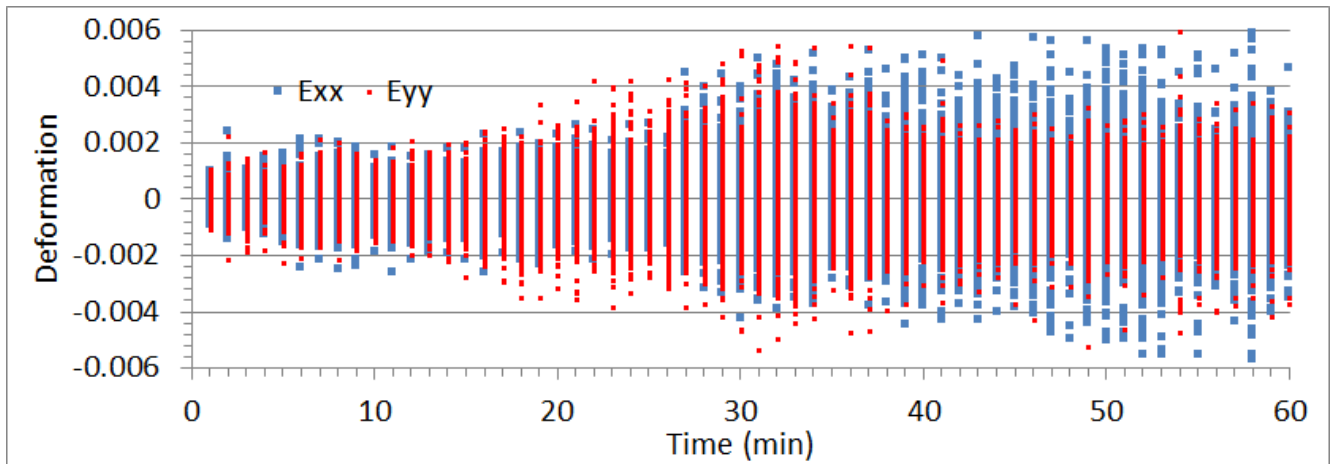
(b)

Figure 7: Example of horizontal (U_x) and vertical (U_y) displacements evolution of all subsets versus time (on the left) and vector plot after 1 hour (on the right), showing 2-dimensional displacements at 20°C (a) and at 1200°C (b). DIC Calculations performed for subset size of 128×128 pixels and spacing of 64×64 pixels on B_SiC_50-100.

Figure 8 presents the evolution of horizontal and vertical deformations versus time during stability test. At 20°C, strain values are small because displacements are small. At 1200°C, rigid body movement like this one shown Figure 7b, does not influence these data. As displacements are larger than the ones at room temperature, strain values are consequently larger. We can observe that strain fluctuations increase from 20 min, but it is beyond the duration to realize the mechanical test. Therefore, deformation values until 20 min will be also selected later as an interesting parameter for comparison of all investigated speckle patterns. In addition, both components of strain exhibiting a same trend, only horizontal strain will be retained for this later comparison.



(a)



(b)

Figure 8. Horizontal and vertical deformations calculated on overall sample, for subset size 128x128 pixels and spacing 64x64 pixels, during stability test (60 min of dwell) at 20°C (a) and at 1200°C (b).

4-3. Influence of DIC parameters and image processing

4.3.1. Low pass filter

Low pass filter (Gaussian filter with a size of 3x3 pixels) is used to decrease measurement uncertainty. In the recorded images, the standard deviation of the noise (σ_n) was about 2 grey levels for all studied cases. This value has been calculated within a uniform area of the image (no local gradient) out of the sample surface (for example on jaws). The main observed effect of the low pass filter is thus to decrease σ_n by a factor close to 2 (σ_n value becoming thus close to 1). Nevertheless, in the same time, applying such low pass filter also slightly blurs the images which is revealed by lower gradients (in fact $\sqrt{\nabla g^2}$ decreases typically by 1.2 in average for all speckles). But globally, as it can be observed on Figure 9 for high temperature tests in the present study, applying such low pass filter deeply improves the quality of the

final strain measurements since standard deviation of strains σ_{Exx} decrease by a value close to 2, for all considered speckles preparation.

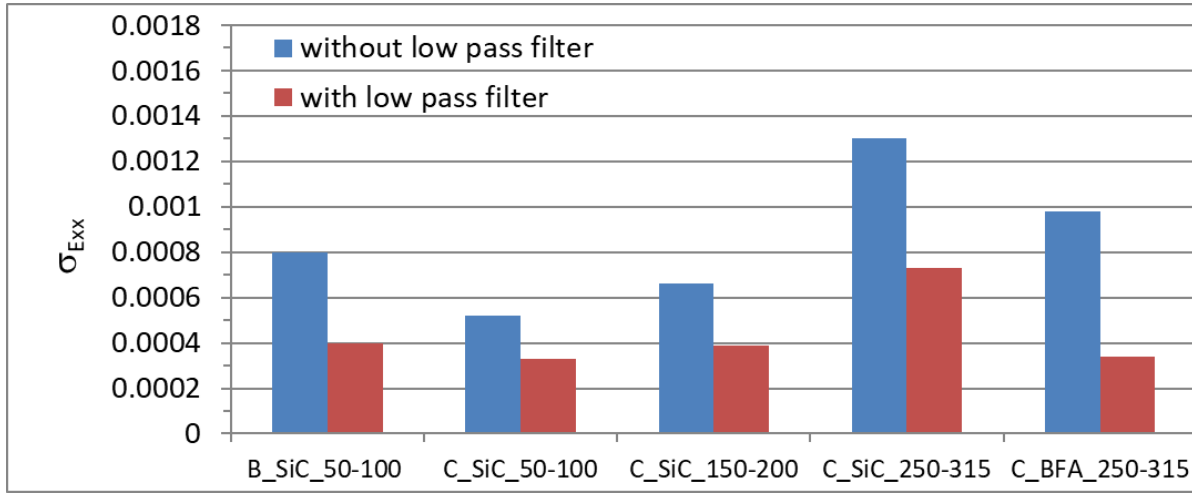


Figure 9. Standard deviation of horizontal strain during 60 minutes of stability test for all samples at 1200°C. Subset size of 128x128 pixels, spacing of 64x64 pixels, with and without additional application of low pass filter.

4.3.2. Subset size

Figure 10 shows strain uncertainty for subset sizes varying from 16 to 128 pixels. One can observe the well-known behaviour of DIC: a decrease subset size leads to an increase of σ_{Exx} for all speckle patterns. Moreover, for a same type of speckle (C_SiC with 3 different grain sizes), the influence of speckle size can be highlighted: lower speckle size leads to more accurate strain measurements (in the investigated range). This observation is in accordance with general recommendations concerning speckle grain size, which should be small enough to provide high spatial resolution and big enough to avoid aliasing [20,41]. In our investigations, the best performance is obtained for C_SiC_50-100 and the worst one for C_SiC_250-315.

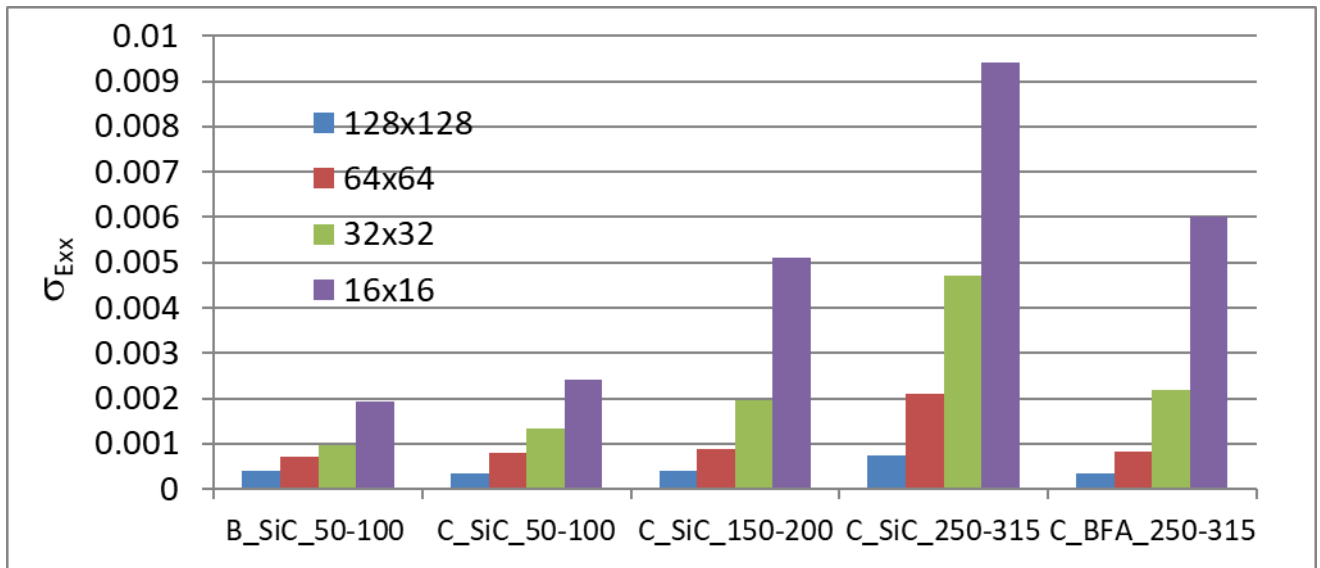


Figure 10. Standard deviations of deformation in horizontal direction “ σ_{Exx} ” for 60 pictures acquired: at 1200°C during one hour of measurement (calculations performed using low pass filtering). Influence of subset size for a same spacing of 64x64 pixels.

4.3.3. Reduction of picture size

For the analysis of one full image (6576 x 4384 pixels), the 2P-DIC computation time is about 5 minutes (on a workstation 32 cores 2.77 GHz). This duration becomes one week for a full test with 2000 images. So, it appears very important for us to decrease the computation time knowing that a series of several specimens have usually to be tested. The size of the speckle is quite large (10 pixels in the smallest case) so, it has been decided to test the influence of a reduced image size by a factor of 4 (image post-processing after recording: averaging 4 pixels to 1 pixel) on the measurement uncertainty σ_{Exx} . In this case, the sampling of the speckle remains acceptable (5 pixels). It should be noticed here that, in order to keep all geometrical factors at the same scale (from sample perspective), this reduction of picture size has been systematically

associated to a reduction of subset size and of strain gauge length (same spacing) in the similar proportion.

As a first result (Figure 11), one can observe that, for all speckle patterns, σ_{Exx} after image size reduction is close to the value for full-size images. This result is described by formula 5: a decrease by a factor two of strain measurement gauge length L_0 (in pixel) is balanced by a decrease close to two of the value of displacement uncertainty σ_{Ux} (in pixel). In fact, this important result could be modeled, in first approximation, by formula 4: σ_{Ux} decreases because the process of image size reduction acts here as a noise reduction operation like a low pass filtering (σ_n is divided by 2.2 and becomes close to 0.9 grey levels in Table 4). In addition,

as indicated in Table 4 (column 3 versus 1), the term $\left[m \cdot \sqrt{\nabla g^2} \right]$ decreases by 1.4 for example, in the case of B_SiC_50-100). In fact, the subset size m is exactly divided by two by the image size reduction while the gradient level $\sqrt{\nabla g^2}$ is multiplied by about 1.5 (grey levels are slightly modified by averaging 4 pixels to 1 pixel, while the pitch of derivation is exactly divided by two). Finally, in the case of B_SiC_50-100, the displacement uncertainty is theoretically divided by 1.6 (2.2/1.4). For the other investigated speckles, this theoretical value can vary from 1.6 to 2 (from value in Table 4). To resume, from theoretical formulation, this demonstrates that the applied image reduction should not affect too much strain accuracy σ_{Exx} at the end. And this is more or less confirmed by obtained results presented in Figure 11.

One can notice that applying the size reduction, and then the low pass filter, together finally do not improve measurement uncertainty as shown in Figure 11. It can be explained by value reported in table 4 (column 4) because the term $\left[m \cdot \sqrt{\nabla g^2} \right]$ decreases more quickly, in this

case, than the noise ($\sigma_n = 0.7$ grey level with low pass filter in comparison to 0.9 before filtering).

Compared to the ideal solution consisting in using full-size images combined with low pass filtering, the uncertainty $\sigma_{E_{xx}}$ using resized images without filter are of course about two time larger (Figure 11). Nevertheless, taking into account the important reduction in calculation time, it appears sufficient for the present study dedicated to crack monitoring. So, as a very important conclusion for our experimental conditions at high temperature, it appears that the solution to reduce image size (decreasing resolution to 0.028 mm/pixel by averaging 4 pixels to 1 pixel) without applying any additional filtering leads, on the one hand, to affect only slightly the uncertainty $\sigma_{E_{xx}}$ and, on the other hand, to decrease significantly calculation times (typically by a factor 10).

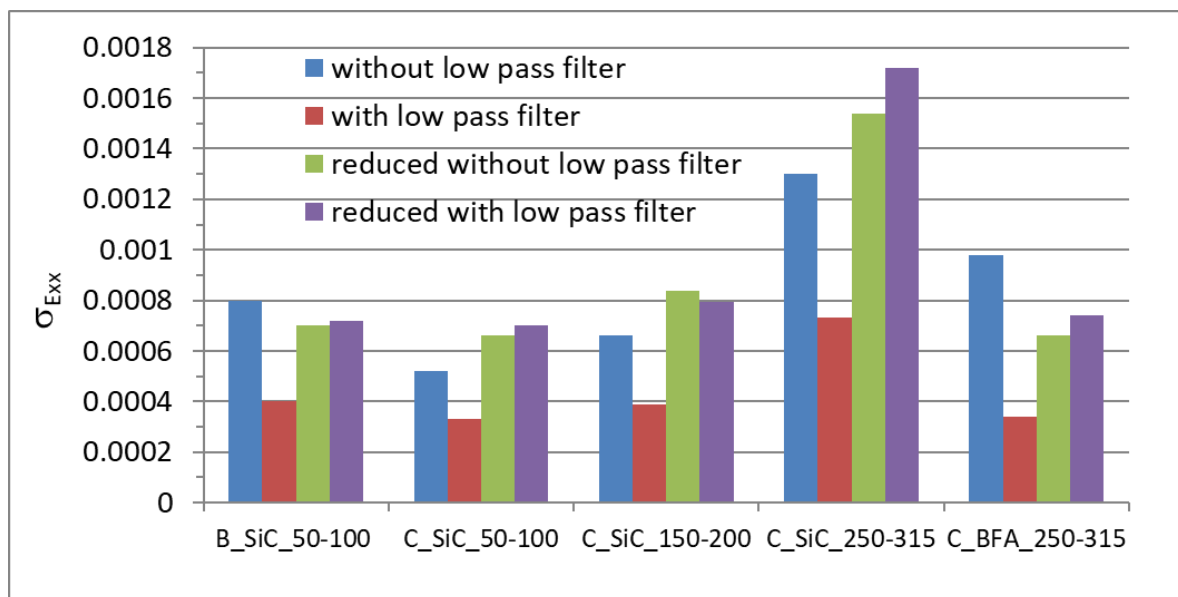


Figure 11. Influence of image resolution on standard deviation of horizontal deformation. Parameters of DIC calculation: subset 128x128 pixels and spacing of 64x64 pixels for initial images and subset 64x64 pixels and spacing of 32x32 pixels for reduced images.

Table 4: Effect of resizing image or/and applying low pass filter on the two major terms

of equation 4 (numerator: noise σ_n - denominator: term $\left[m \cdot \sqrt{\nabla g^2} \right]$).

	Full image without filter d=128 pixels (ref.)	Full image with low pass filter d=128 pixels	Resized image without filter d=64 pixels	Resized image with low pass filter d=64 pixels
noise (σ_n)				
Average for all speckles	2.0	1.0 (ref. / 2.0)	0.9 (ref. / 2.2)	0.7 (ref. / 2.9)
term $\left[m \cdot \sqrt{\nabla g^2} \right]$				
B_SiC_50-100	422	358 (ref. / 1.2)	307 (ref. / 1.4)	243 (ref. / 1.7)
C_SiC_50-100	589	513 (ref. / 1.1)	378 (ref. / 1.6)	307 (ref. / 1.9)
C_SiC_150-200	525	435 (ref. / 1.2)	416 (ref. / 1.3)	333 (ref. / 1.6)
C_SiC_250-315	448	384 (ref. / 1.2)	352 (ref. / 1.3)	282 (ref. / 1.6)
C_BFA_250-315	448	371 (ref. / 1.2)	339 (ref. / 1.3)	262 (ref. / 1.7)

4.3.4. Choice of 2P-DIC strain threshold

Previous DIC results were obtained with square subsets, as usually used in order to have the same uncertainty in all directions. For 2P-DIC technique, it is usually much more judicious to choose rectangular subsets with a length (highest side) in the direction perpendicular to the expected cracks (for example 64x16 pixels with a spacing of 32x8 pixels), in order to achieve a better cracks detection [15, 33] when local pseudo strain value (within each subset) will be higher than a given threshold value ε_{Thres} . In our case, during later Brazilian tests, the cracks expected within the loaded sample will be mostly vertical, thus, the highest side (length) of the subsets have been voluntary set horizontally. In order to account for such adjustments, strain fields have been recalculated (for each previous test) with those new horizontal rectangular subsets to be able to predetermine accurately the value of strain threshold ε_{Thres} that will be required later for 2P-DIC process to detect local cracks. As a very good

representative example of results, Figure 12 plots the histogram of horizontal pseudo strains within such rectangular subsets for C-SiC_50-100 case during the 60 minutes of stability test (with a very small preload of 50 N for which one can assume that no local cracks can take place). Thus, the value of pseudo strain threshold ϵ_{Thres} (used for later cracks detection) could be predetermine at the value corresponding to the maximum uncertainty (without any cracks in such case) in order to avoid too noisy results (over detection of non-existing cracks). Graph of Figure 12 being in semi logarithm scale, one can assume that a pseudo strain threshold ϵ_{Thres} at 0.0035 could be a reasonable value with less than 10 subsets (over 700000 subsets) with a crack detected inside. A similar approach has been applied for all considered speckles and leads to Figure 13 providing pseudo strain threshold ϵ_{Thres} (with less than 10 subsets with a crack detected inside) for each sample surface preparation. This graph clearly demonstrates that, the smallest values of pseudo strain threshold (lower than 0.005) are obtained for C_SiC_50-100 and B_SiC_50-100, the other speckle patterns giving significantly higher measurement uncertainties.

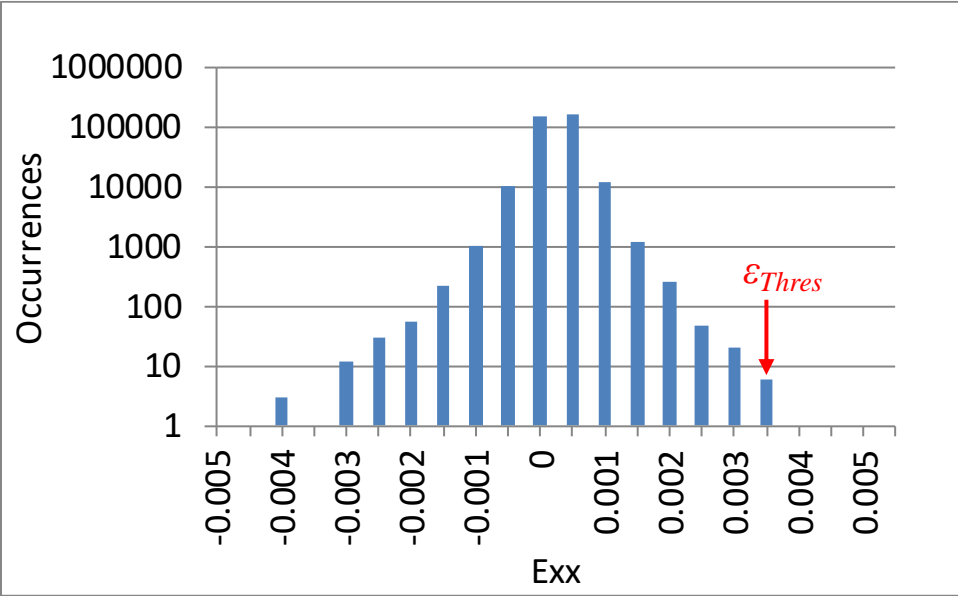


Figure 12. Histogram of Exx for C-SiC_50-100 case during the 60 minutes of stability test (with a very small preload of 50 N for which one can assume that no local cracks can take place).

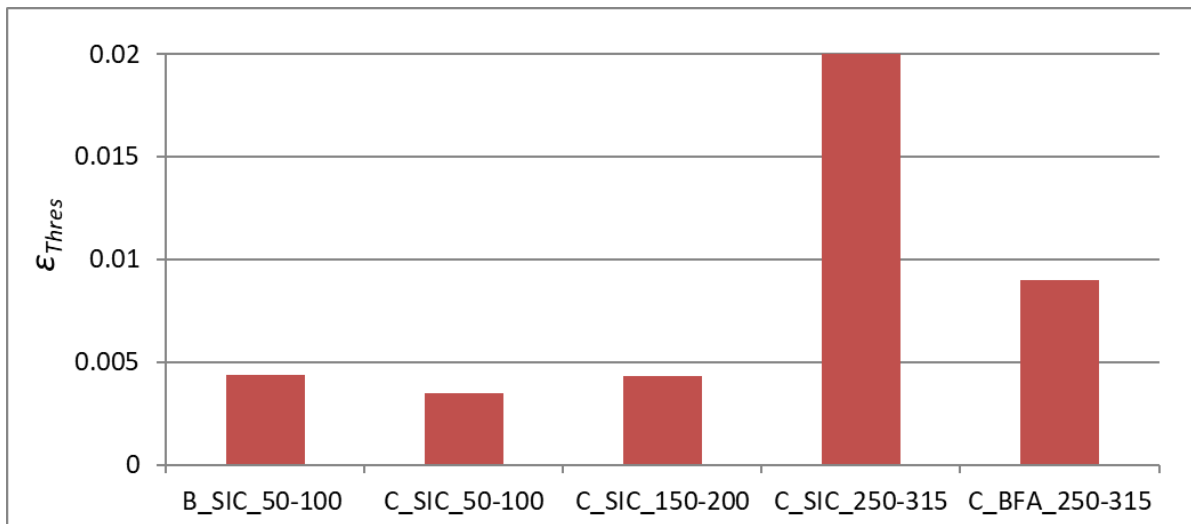


Figure 13. Predetermined value of pseudo strain threshold ϵ_{Thres} (with less than 10 subsets with a crack detected inside) for each considered speckle patterns.

4-4. Application to sample monitoring during Brazilian test at high temperature

All considered speckle pattern preparations being previously fully characterized from DIC numerical treatment point of view in order to reduce final measurement uncertainties, the following section will be then dedicated to the application of such speckle patterns in order to accurately monitor cracks propagation within refractory materials during a mechanical test at high temperature. In the present paper, Brazilian test at 1200°C should be seen as an example of mechanical test that could be monitored thanks to DIC and 2P-DIC with a suitable surface preparation. Of course, the intention of this work is for sure to apply later a similar procedure

to other kind of tests that are also very important to characterise the high temperature behaviour of refractory materials: for example, wedge splitting tests (41). In addition, the case of an alumina-spinel fired brick, that has been considered in the present paper, should be seen as an example of refractory materials that could be interesting to investigate in more details later, considering its large application in steel making (for steel ladle lining). Having these two important contextual points in mind and the main purpose of the present paper being on optimisation of experimental procedure for crack monitoring by DIC and 2P-DIC within high temperature condition, analyse of results presented in this section (and discussion) will be focused exclusively on this specific procedural aspect and not on material aspects.

4.4.1. Overview on typical load-displacement curves during a Brazilian test at 1200°C

Before analysing results obtained by DIC and 2P-DIC, Figure 14 presents all the load-displacement curves obtained for the investigated samples (same material and same geometry) prepared with the different considered speckle patterns studied in the first part of this paper. As a reminder, in order to remove the effects of contacts between sample and jaws, displacement ΔU has been measured directly on the sample by DIC between two area placed at the top and at the bottom of sample close to the jaws. Results exhibit some discrepancies from one sample to the others. These discrepancies could of course not be attributed to the difference of speckle preparations but simply results from the natural heterogeneity of such refractory materials with large grains (typically up to several mm). For such refractory materials, it is quite common to not obtain exactly same stress-strain curves when samples are loaded during mechanical tests, especially at high temperature. Nevertheless, as displayed in Figure 14, a rather linear load-displacement dependence can be classically observed in the very first stage of loading for all samples (at least until 0.01 mm of displacement ΔU). After this first stage, the behaviour becomes non-linear highlighting the occurrence of a pseudo

plastic (or/and damageable behaviour) until a plateau can be reach (with an almost constant value of load). Such a plateau (or in some case a decrease) corresponds usually to the step during which a localisation of damage in the central part of the sample leads to a macrocracks indicating the starting point of final rupture of the sample. After this rupture occurrence (end of the plateau or minimum of the curve), a new increase of load could be observed. But this final part of the curve usually simply corresponds to the loading in compression of the two separated half discs and, thus have absolutely no meaning from materials science point of view.

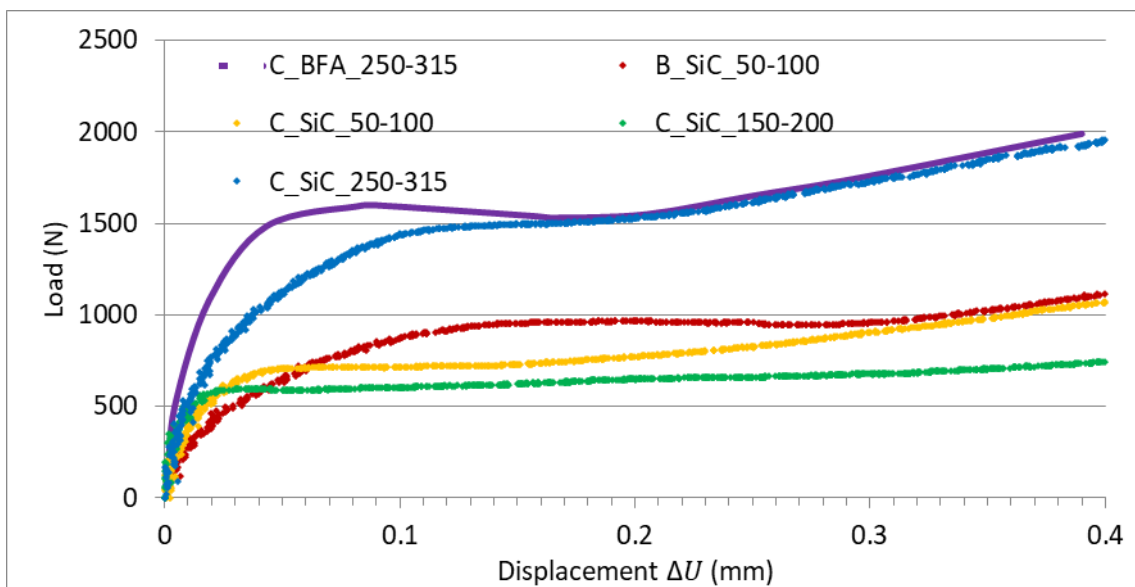
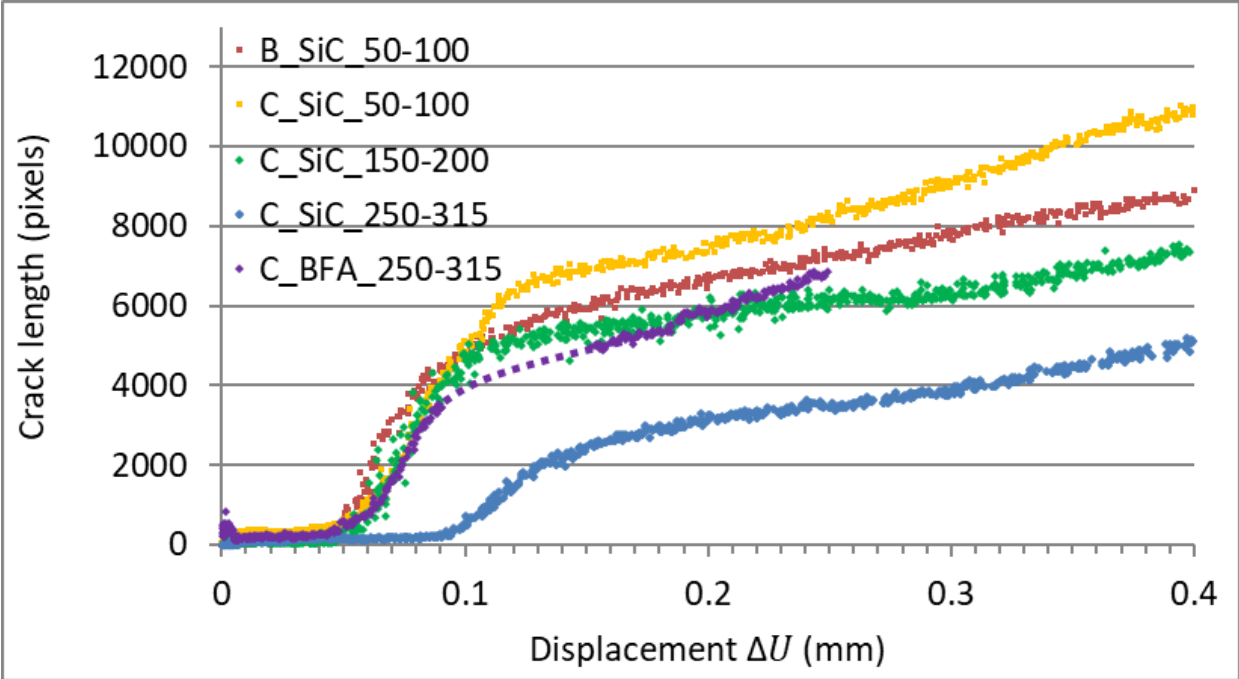


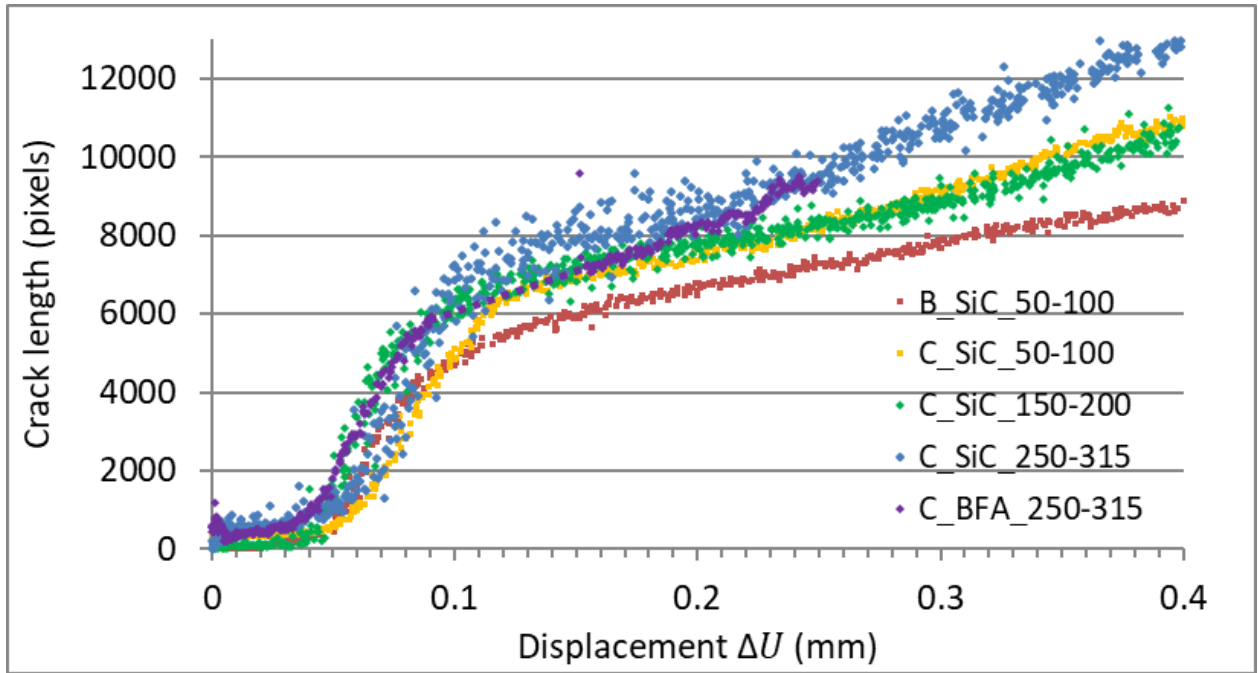
Figure 14: Load-displacement curves during Brazilian test at 1200°C for the different considered samples (displacement ΔU measured directly on the sample by DIC between two area placed at the top and at the bottom of sample close to the jaws).

Figure 15 reports crack length evolutions, on the one hand, in Figure 15a considering the different optimal values of ε_{Thres} (see Figure 13) calculated from maximal strain uncertainties of each speckle pattern and, on the other hand, in Figure 15b considering a uniform value of $\varepsilon_{Thres}=0.005$ corresponding to a reasonable suitable level for optimal speckle patterns with

small grain size (for B-SiC_50-100 and C-SiC_50-100). As shown Figure 15a, all curves exhibit a rather similar noise level. This result is extremely logic since ϵ_{Thres} has been adapted in this case to metrological performance of each speckle, but the level of crack lengths can be significantly different from one curve to the other, especially for C_SiC_250_315. In fact, for this speckle with a rather large grain size, the optimal value of ϵ_{Thres} (with low noise level) is too high to detect cracks with a small opening: the crack length is thus largely underestimated. For the other speckle patterns which have rather close optimal values of ϵ_{Thres} , the 2P-DIC numerical treatment leads to rather same starting point of cracking and rather close values of crack lengths despite a small dispersion due to the variability from one sample to the other. With a uniform value of $\epsilon_{Thres}=0.005$ (Figure 15b), the 2P-DIC numerical treatment leads to rather similar crack lengths but the obtained curves exhibit different noise levels, depending on metrological performance of each speckle pattern (as explained in the previous section).



(a)



(b)

Figure 15: Crack length-displacement curves during Brazilian test: influence of different speckle grain size, (a) with ε_{Thres} adapted at each speckle pattern (b) with an uniform value of $\varepsilon_{Thres}=0.005$

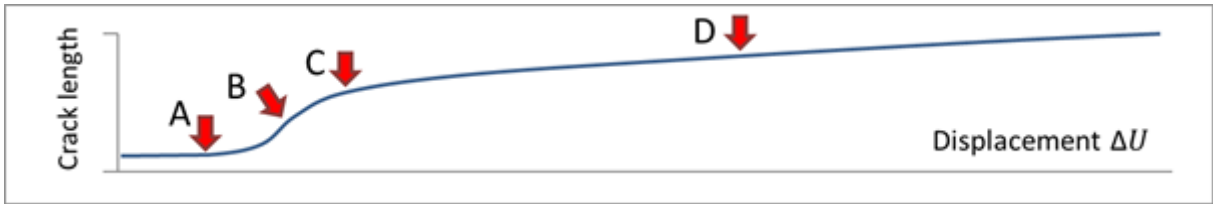
For more precise estimation of this noise in each case, dispersion in crack length values have been calculated as standard deviation of the difference between real values of crack length and local linear tendency of the curve within a specific range of displacement ΔU : at the beginning of the test (ΔU from 0 to 0.04 mm) and at the end of the test (ΔU from 0.2 to 0.4 mm). Such obtained dispersions in crack length are reported in Table 4. It appears that, in each case, the dispersion in crack length is higher at the end of the test. This result could be explained by a degradation of the speckle pattern (peeling off of surface preparation: cement and/or grains) when local strain level becomes too high and also especially when a crack appears locally. A similar trend has in fact also been observed at room temperature: dispersion in crack length being close to 0 at the beginning of the test and reaching 35 pixels (1mm) at

the end. For tests managed at 1200°C and presented here, the largest dispersion in crack length is logically observed for C_SiC_250-315 speckle pattern with the biggest grain size (some subsets may lack contrast when grains are too big for the chosen subsets). On the contrary, speckle patterns with small grain size (B_SiC_50-100 and C_SiC_50-100) exhibit the lowest dispersion in crack length.

Table 4. Dispersion in crack length measurement at the beginning of the test (ΔU from 0 to 0.04 mm) and at the end of the test (ΔU from 0.2 to 0.4 mm)

	Dispersion in crack length in pixel (and in mm)	
	Beginning of the test (ΔU from 0 to 0.04 mm)	End of the test (ΔU from 0.2 to 0.4 mm)
B_SiC_50-100	10.5 (0.3 mm)	94 (2.6 mm)
C_SiC_50-100	21.8 (0.6 mm)	120 (3.36 mm)
C_SiC_150-200	65.6 (1.8 mm)	278 (7.8 mm)
C_SiC_250-315	143 (4 mm)	367 (10.3 mm)
BFA_SiC_250-315	45 (1.3 mm)	130 (3.7 mm)

As a key final result for the different investigated speckle patterns, Figure 16 highlights the cracks paths detected by the 2P-DIC analysis (based on previously optimised parameters) at four key loading states: A just at main crack initiation, B at inflection point of main crack growing, C when main crack length reach a plateau (final stage of main central crack propagation) and D when the two rather separated half discs began to be loaded in compression (no more meaning from materials science point of view). This final result confirms the performance of each speckle pattern in term of accuracy of crack length determination. Patterns with a small optimised ε_{Thres} allow to see most of details, in particular cracks with a small opening. In contrast, patterns with a big ε_{Thres} give only the main crack.



	A	B	C	D
B_SiC_50-100				
C_SiC_50-100				
C_SiC_150-200				
C_SiC_250-315				
C_BFA_250-315				

Figure 16: Pictures of highlighted cracks path determined by 2P-DIC numerical treatment at four key loading states during Brazilian test at 1200°C with an optimal value of ϵ_{Thres} adapted to each speckle pattern.

4.4.2. Measurement bias of imposed displacement

The previous results presented in this paper have been obtained using the imposed displacement ΔU measured directly on the sample by DIC between two areas placed at the top and at the bottom of sample close to the jaws. This method using DIC is not commonly used in the area of refractory mechanical testing. An alternative, but more conventional method is to use the displacement imposed by the crosshead of the testing machine. Figure 17 gives the same results than Figure 15b but with this crosshead displacement. As a consequence, much larger horizontal shifts can be observed between the different curves in Figure 17 in comparison with the ones observed in Figure 15b. With such representation of the experimental data, results are in fact greatly affected by the contact mechanical behaviour between external cylindrical surface of the sample and cylindrical surface of the loading jaws. Even if the geometry of this loading jaws has been optimised (slightly larger diameter in comparison to the sample) in order to reduce local compression, the contact mechanical behaviour is in fact not perfectly reproducible from one test to the other, and, in any case, leads to a non-linear loading of the disk shape sample (inducing some non-reproducible delay in loading at the very beginning of each test). It is thus much better to measure this imposed displacement ΔU directly on sample side by DIC near the jaws as managed in the present study. This way allows to avoid introducing measurement bias which could have significant consequences in the interpretation of the fracture behaviour, as already shown in another study [43].

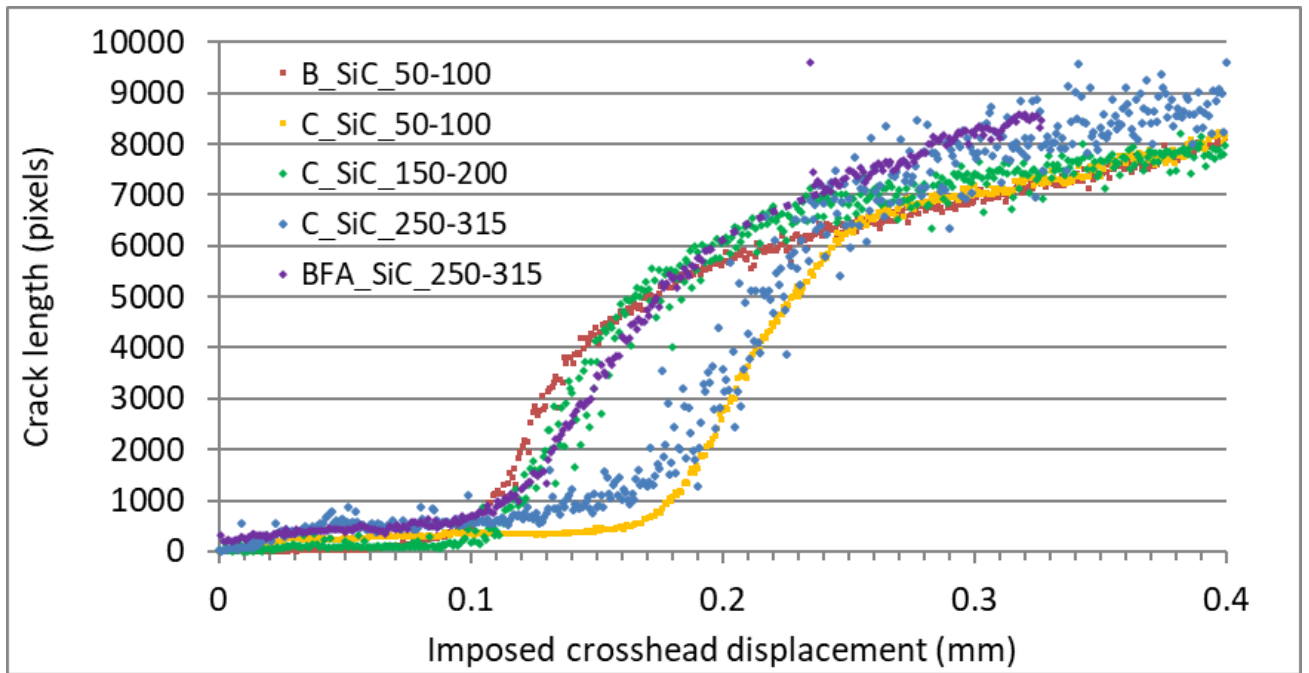
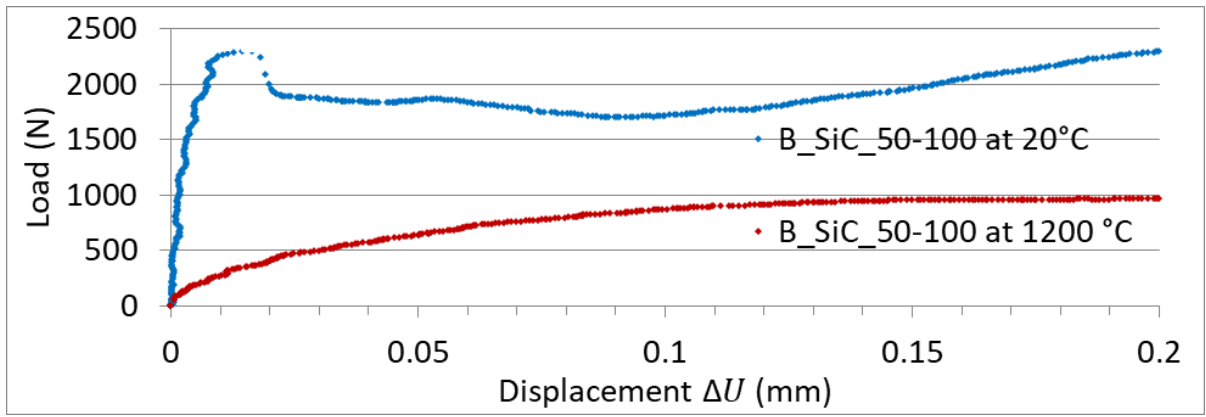


Figure 17: Crack length-displacement curves during Brazilian test with an uniform value of $\epsilon_{Thres}=0.005$ and imposed crosshead displacement.

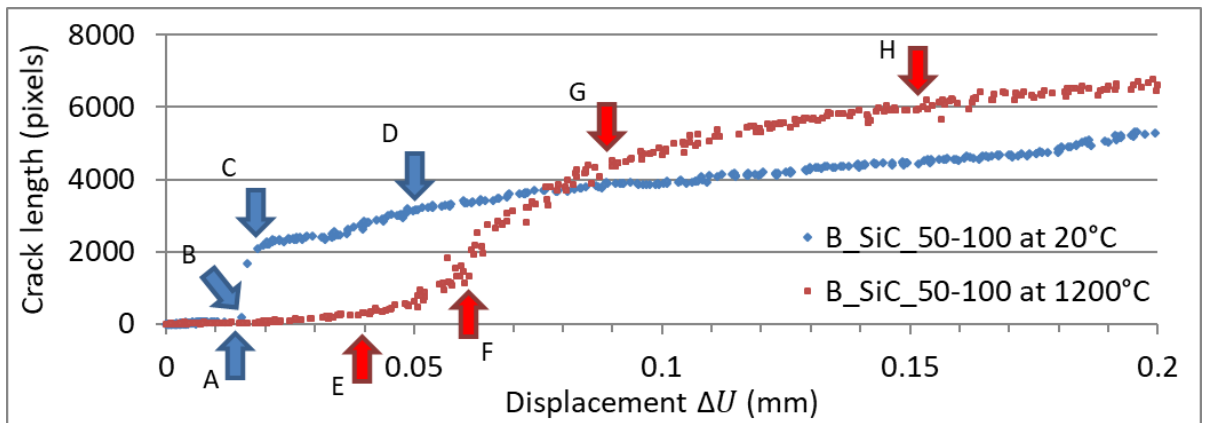
4.4.3. Temperature dependent fracture behaviour

The global aim of the present study was to define an optimal speckle patterns preparation for later in-depth investigations of mechanical behaviour of refractory materials versus temperature. It was thus interesting to finally present a short analyse of significant differences that could be observed, versus temperature, in crack propagation within this investigated alumina-spinel material. From results presented in previous sections, two samples have been prepared only with B_SiC_50_100 as an optimal speckle pattern. Figure 18 presents load-displacement curves (a), crack length-displacement curves (b), and pictures of cracks path (c) at four loading states (as previously defined) during a Brazilian test in two extreme experimental conditions: room temperature and 1200 C. It should be noted that results have

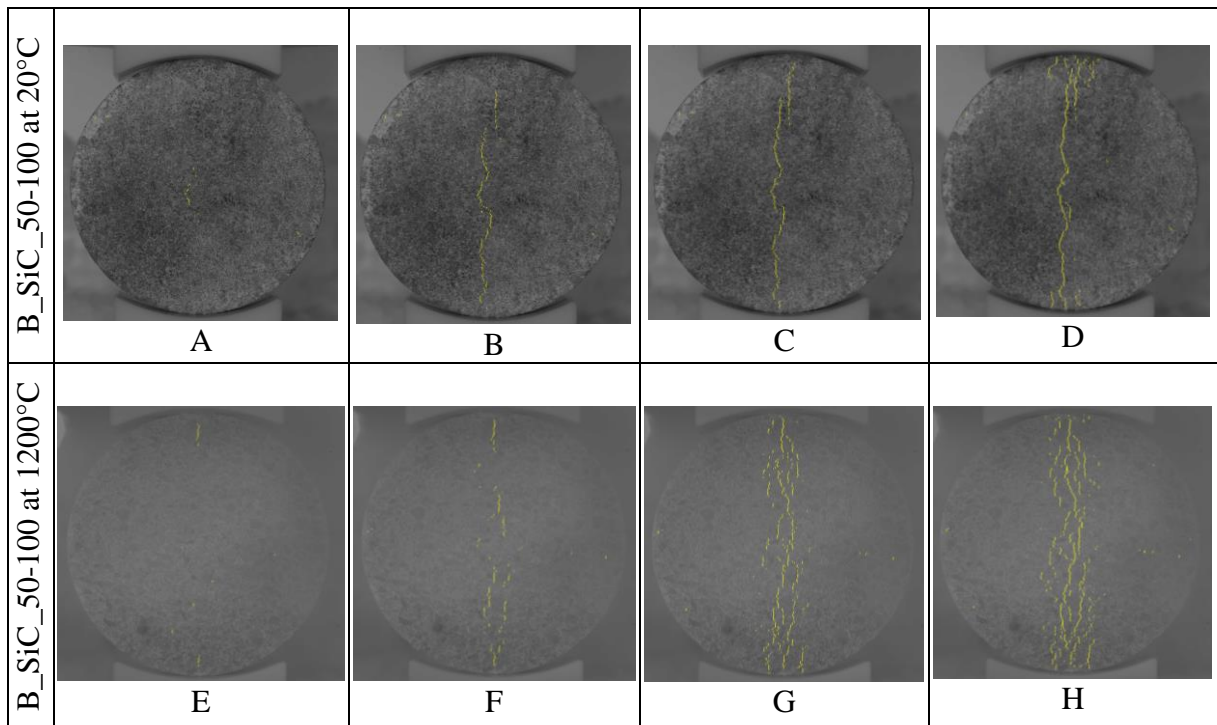
been obtained with an optimized ε_{Thres} for each series of images ($\varepsilon_{Thres} = 0.003$ at 20°C and $\varepsilon_{Thres} = 0.005$ at 1200°C). At 20°C , crack length increases suddenly (points A, B and C being very close to each other), leading to a very brittle fracture (rupture within 3 seconds with a very low level of displacement $\Delta U \sim 0.015$ mm). This fracture rather occurred during linear increase of load, corresponding to an important storage of elastic energy, which led to a sudden failure, with only a single crack crossing the middle of the sample. At 1200°C , crack length increases much more progressively (points E, F and G being very far to each other), leading to a non-brittle fracture (rupture needing more time with larger level of displacement $\Delta U \sim 0.1$ mm). This fracture thus takes place with a much lower storage of elastic energy, which leads to a progressive failure, with numerous small cracks within the central part of the sample. This fracture process at high temperature indicates much larger energy dissipation phenomena, resulting in progressive rupture.



(a)



(b)



(c)

Figure 18. (a) Load-displacement (b) Crack length-displacement curves (c) Pictures of cracks at four loading states during Brazilian test at 20°C and 1200°C

5. Conclusion

The aim of this work was to develop a robust experimental protocol in order to later study fracture behaviour of refractory materials at high temperature by using Digital Image Correlation. In that purpose, an experimental device has been setup integrating different key points (well-designed alumina jaws to reduce stress concentration during mechanical loading, suitable speckle pattern and dedicated lightning for an improved grey level contrast on sample surface, specific blue band pass filter to remove infrared radiations from the furnace) allowing to reduce undesirable phenomena that could be induced by high temperature and to define optimised experimental conditions for images acquisition. In particular, a special attention has been paid to the procedure of sample surface preparation based on different ceramic powders (type and grain size) in order to obtain a speckle pattern resistant at 1200°C that could be very suitable for accurate measurements by DIC and 2P-DIC. Grey levels distribution of recorded images linked to each investigated speckle pattern (distribution, gradient, speckle size) have been deeply characterized for a full comparison of their performance in numerical treatments. The study of strain uncertainty allows us to define the best speckle patterns: B_SiC_50-100 and C_SiC_50-100. In fact, among these two patterns, in the future, B_SiC_50-100 will be preferred because the sample preparation is easier. By studying the influence of images pre-processing (images filtering and/or images size reduction) and of some DIC parameters, a very good compromise has been found between a good accuracy/resolution of final results and a reasonable processing duration. This experimental procedure will thus be adequate for

early detection of the cracks and their length measurement by 2P-DIC in refractory materials during mechanical loading at high temperature. As an illustration of such investigations, the best procedure of sample surface preparation (B_SiC_50-100) has been applied to compare the fracture behaviour of an alumina-spinel refractory material between two extreme experimental conditions (20 °C and 1200 °C) proving the pertinence of the optimized speckle pattern protocol within a large temperature range. The experimental protocol developed in the present study could thus be used later to deeply characterize, by DIC and 2P-DIC, the mechanical behaviour of different refractory materials (by Brazilian tests or by wedge splitting test) in order to compare their performance in high temperature applications (up to 1200°C and probably higher).

6. Acknowledgements

This work was supported by European Union's Horizon 2020 research and innovation programme under the Marie Skłodowska-Curie grant agreement No 764987 (project ATHOR: Advanced THermomechanical multiscale modelling of Refractory linings). Authors are also very grateful to RHI Magnesita for providing Alumina Spinel refractory materials, St. Gobain for providing SiC grains and Imerys for providing Brown Fused Alumina grains (both used for speckle patterns preparation).

7. References

[1] Chu TC, Ranson WF, Sutton MA, Peters WH Applications of digital-image-correlation techniques to experimental mechanics. *Exp Mech* 1985 25(3):232–244

[2] Bruck HA, McNeill SR, Sutton MA, Peters WH Digital image correlation using Newton–Raphson method of partial differential correction. *Exp Mech* 1989 29(3):261–267

- [3] Choi S, Shah SP Measurement of deformations on concrete subjected to compression using image correlation. *Exp Mech* 1997 37(3):307–313
- [4] Pan B, Kemaq Q, Xie H, Asundi A Two-dimensional digital image correlation for in-plane displacement and strain measurement: a review. *Meas Sci Technol* 2009 20(6):1–17
- [5] Sutton MA, Helm JD, Boone ML Experimental study of crack growth in thin sheet 2024-T3 aluminum under tension–torsion loading. *Int J Fract* 2001 109(3):285–301
- [6] Jin H, Lu WY, Haldar S, Bruck HA Microscale characterization of granular deformation near a crack tip. *J Mech Sci* 2011 46:6596–6602
- [7] Mathieu F, Aimedieu P, Guimard J-M, Hild F Identification of interlaminar fracture properties of a composite laminate using local full-field kinematic measurements and finite element simulations. *Compos A* 2013 49:203–213
- [8] Réthoré J, Estevez R Identification of a cohesive zone model from digital images at the micron-scale. *J Mech Phys Solids* 2013 61:1407–1420
- [9] Zhang Q, Zhao J Determination of mechanical properties and full-field strain measurements of rock material under dynamic loads. *Int J Rock Mech Min Sci* 2013 60:423–439
- [10] Tracy J, Daly S, Sevener K Multiscale damage characterization in continuous fiber ceramic matrix composites using digital image correlation. *J Mech Sci* 2015 50:5286–5299
- [11] Belrhiti Y, Pop O, Germaneau A, Doumalin P, Dupré J-C, Harmuth H, Huger M, Chotard T Investigation of the impact of micro-cracks on fracture behavior of magnesia

products using wedge splitting test and digital image correlation. *J Eur Ceram Soc* 2015
35(2):823–829

[12] Dupré J. C., Doumalin P., Hussein H. A., Germaneau A. and Brémand F., Displacement Discontinuity or Complex Shape of Sample: Assessment of Accuracy and Adaptation of Local DIC Approach. *Strain* 2015 51(5): 391–404

[13] Poissant J, Barthelat F A novel, “subset splitting” procedure for digital image. *Exp Mech* 2010 50:353–364

[14] Sousa AMR, Xavier J, Morais JLL, Filipe VMJ, Vaz M Processing discontinuous displacement fields by a spatio–temporal. *Opt Laser Eng* 2011 49:1402–1412

[15] Dupré J-C, Doumalin P., Belrhiti Y., Khlifi I., Pop O., Huger M., Detection of cracks in refractory materials by an enhanced digital image correlation technique. *J Mech Sci* 2018
53(2): 977–993

[16] Viguié J, Dumont P, Mauret E, Rolland du Roscoat S, Vacher P, Desloges I, Bloch JF Analysis of the hygroexpansion of a lignocellulosic fibrous material by digital correlation of images obtained by X-ray synchrotron microtomography: application to a folding box board. *J Mech Sci* 2011 46:4756–4769

[17] Kravchenko OG, Kravchenko SG, Casares A Digital image correlation measurement of resin chemical and thermal shrinkage after gelation. *J Mech Sci* (2015) 50:5244–5252

[18] Rethoré J, Hild F, Roux S Extended digital image correlation with crack shape optimization. *Int J Numer Methods Eng* 2008 73:248–272

- [19] Wang Y, Sutton M, Bruck H, Schreier H Quantitative error assessment in pattern matching: effects of intensity pattern noise, interpolation, strain and image contrast on motion measurements. *Strain* 2009 45:160–178.
- [20] Bornert M, Brémand F, Doumalin P, et al. Assessment of digital image correlation measurement errors: Methodology and results. *Exp Mech.* 2009;49(3):353-370
- [21] Barranger Y, Doumalin P, Dupré J-C, Germaneau A Strain Measurement by Digital Image Correlation: Influence of Two Types of Speckle Patterns Made from Rigid or Deformable Marks. *Strain* 2012 28(5):357–365.
- [22] Amiot F, Bornert M, Doumalin P, et al. Assessment of digital image correlation measurement accuracy in the ultimate error regime: Main results of a collaborative benchmark. *Strain* 2013 49(6):483–496
- [23] Pan B, Xie H, Wang Z, Qian K, Wang Z Study on subset size selection in digital image correlation for speckle patterns *Opt. Express* 2008 16(10):7037–7048
- [24] Pan B. Bias error reduction of digital image correlation using Gaussian pre-filtering. *Opt Lasers Eng.* 2013 51(10):1161-1167
- [25] Zhou Y, Sun C, Song Y, Chen J Image pre-filtering for measurement error reduction in digital image correlation *Optics and Lasers in Engineering* 2015 65: 46-56
- [26] Bing Pan DW. High-temperature digital image correlation method for full-field deformation measurement at 1200 °C. *Meas Sc. Tech.* 2010 22(1).

- [27] Xiang Guo JL. High-temperature digital image correlation method for full-field deformation measurement captured with filters at 2600°C using spraying to form speckle patterns. *Opt. Eng.* 2014 53(6).
- [28] Leplay P., Lafforgue O., Hild F. Analysis of Asymmetrical Creep of a Ceramic at 1350°C by Digital Image Correlation. *Journal of the American Ceramic Society* 2015 98(7):2240-2247.
- [29] Koohbor B., Valeri G., Kidane A., Sutton M. A. Thermo-mechanical Properties of Metals at Elevated Temperatures. *Advancement of Optical Methods in Experimental Mechanics* 2016(3):117-123.
- [30] Valeri G., Koohbor B., Kidane A., Sutton M. A. Determining the tensile response of materials at high temperature using DIC and the Virtual Fields Method. *Opt Lasers Eng.* 2017(91):53-61.
- [31] Lyons J.S., Liu J., Sutton M.A. High-temperature Deformation Measurements Using Digital-image Correlation. *Exp. Mech.* 1996 36(1):64-70.
- [32] Novak M. and Mark D. High-temperature materials testing with full-field strain measurement: Experimental design and practice. *Review of Scientific Instruments* 2011:82(11)
- [33] Dusserre G., Nazaret F., Robert L., Cutard T., Applicability of image correlation techniques to characterize asymmetric refractory creep during bending tests. *J. of the European Ceramic Society* 2013(33):221-231.

- [34] Khelifi I., Pop O., Dupré J-C, Doumalin P., Huger M., Investigation of microstructure-property relationships of magnesia-hercynite refractory composites by a refined digital image correlation technique, *J. of the European Ceramic Society* 2019 39(13):3893-3902
- [35] Bornert M., Doumalin P., Dupré J. et al. Assessment of Digital Image Correlation Measurement Accuracy in the Ultimate Error Regime: Improved Models of Systematic and Random Errors. *Exp Mech* 2018 58:33–48
- [36] Heilbronner R. the autocorrelation function: an image processing tool for fabric analysis, *Tectonophysics* 1992 212(3–4):351-370
- [37] Doumalin P., Bornert M., Crépin J. Caractérisation de la répartition de la déformation dans les matériaux hétérogènes *Mécanique & Industries* 2003 4(6):607-617,
- [38] ASTM Subcommittee: D18.12. Standard Test Method for Splitting Tensile Strength of Intact Rock Core Specimens. 2001.
- [39] Zavaliangos A., Laptev A., eds. Recent Developments in Computer Modeling of Powder Metallurgy Processes. Vol 176. IOS Press, Ohmsha, NATO Scientific Affairs Division; 2001.
- [40] Markides Ch.F., Kourkoulis S.K. The influence of jaw's curvature on the results of the {Brazilian} disc test. *J. of Rock Mechanics and Geotechnical Engineering* 2016 8(2):127-146.
- [41] International Digital Image Correlation Society, Jones, E.M.C. and Iadicola, M.A. (Eds.) (2018). A Good Practices Guide for Digital Image Correlation. DOI: 10.32720/idics/gpg.ed1
- [42] Doitrand A., Estevez R., Thibault M., Leplay P., Fracture and Cohesive Parameter Identification of Refractories by Digital Image Correlation Up to 1200°C, *Exp Mech* 2020 60:577-590

[43] Belrhiti Y., Gallet-Doncieux A., Germaneau A., Doumalin P., Dupré J-C, Alzina A., Michaud P., Pop O, Huger M, Chotard T Application of optical methods to investigate the non-linear asymmetric behavior of ceramics exhibiting large strain to rupture by four-points bending test J Eur Ceram Soc 2012 32:4073–4081